PROVENANCE AND SEDIMENTOLOGY OF RED CLAY AND LOESS IN NORTHERN CHINA

YUAN SHANG

ACADEMIC DISSERTATION
To be presented, with the permission of the Faculty of Science of the University of Helsinki, for public examination in Auditorium A111, Exactum, Kumpula, on January 19th 2018, at 2 p.m.

DEPARTMENT OF GEOSCIENCES AND GEOGRAPHY A57 / HELSINKI 2018

Cover photo: Anu Kaakinen

Author´s address: Yuan Shang
Division of Biogeosciences
Department of Geosciences and Geography
P.O.Box 64
00014 University of Helsinki, Finland
yuan.shang@helsinki.fi

Supervised by: Docent Anu Kaakinen
Department of Geosciences and Geography
University of Helsinki, Finland

Associate Professor Maarten A. Prins
Department of Earth Sciences
Vrije Universiteit Amsterdam, the Netherlands

Associate Professor Christiaan J. Beets
Department of Earth Sciences
Vrije Universiteit Amsterdam, the Netherlands

Reviewed by: Professor Huayu Lu
School of Geography and Ocean Science
Nanjing University, China

Senior scientist Jan Berend Stuut
Royal Netherlands Institute for Sea Research
the Netherlands
&
MARUM – Center for Marine Environmental
Sciences at Bremen University, Germany

Opponent: Docent Thomas Stevens
Department of Earth Sciences
Uppsala University, Sweden

ISSN-L 1798-7911
ISSN 1798-7911 (print)
ISBN 978-951-51-2939-0 (paperback)
ISBN 978-951-51-2940-6 (PDF)
http://ethesis.helsinki.fi

Unigrafia
Helsinki 2018

This dissertation is the result of a double doctorate program carried out at:

University of Helsinki
Faculty of Science
Department of Geosciences and Geography
Helsinki, Finland
&
Vrije Universiteit Amsterdam
Faculty of Science
Department of Earth Sciences
Amsterdam, the Netherlands

To see a world in a grain of sand
- William Blake

Shang Y., 2018. *Provenance and sedimentology of Red Clay and loess in northern China*. Unigrafia, Helsinki. 45 pages, 7 figures and 1 table.

Abstract

Red Clay and overlying loess-palaeosol sequences are typical for the area in Northern China that is known as the Chinese Loess Plateau (CLP). These primarily aeolian sediments provide one of the best terrestrial archives of Neogene-Quaternary climate change, and their formation has been linked to the uplift of the Tibetan Plateau, the progressive aridification of East Asia and the onset of and changes in the East Asian monsoon. In the present study, the sediment provenance was reconstructed using a combination of analytical techniques that allowed better understanding of the (long-term) shifts in sediment delivery in response to changes in the climate and tectonic evolution.

Zircon U–Pb age spectral and backtrace trajectory modelling of three well-known Red Clay sequences distributed across the CLP revealed spatiotemporal variations in the provenance of late Miocene-Pliocene Red Clay. The results indicate that the Red Clay in the southern and western CLP was mainly derived from the Northern Tibetan Plateau (NTP) and the Taklimakan Desert. In contrast, Red Clay in the northeastern CLP displays a zircon U-Pb age signature of the broad area of the Central Asian Orogenic Belt. In addition, the northeastern Red Clay shows increased contributions from the west around 3.6 Ma, possibly suggesting an intensified westerly wind strength and/or aridity of the NTP and Taklimakan Desert arising from the uplift of the NTP and Tianshan Mountains in the Pliocene. This could also be caused by the onset of enhanced Yellow River drainage in response to the increased NTP denudation since 3.6 Ma.

To further investigate the role of the Yellow River in supplying dust to the Quaternary loess deposits, the sedimentology and source signal of the unique loess-palaeosol sequence of the Mangshan Loess Plateau (MLP) along the lower reach of the Yellow River was investigated by end-member modelling of the loess grain-size records and single-grain zircon U-Pb dating. The results suggest that the Yellow River floodplain north of the MLP has served as a major dust source at least since 900 ka. The sudden change in sedimentology (accumulation rate, grain-size distribution) of the Mangshan sequence above palaeosol unit S2 may have been initiated by a combination of tectonic movements in the Weihe Basin and in the Yellow River floodplain north of the MLP around 240 ka. Subsequent rapid fluvial incision in the northern part of the Weihe Basin resulted in increased sediment flux being transported to the lower reach of the Yellow River. Tectonic movements in the floodplain north of the MLP would have caused a southward migration of the Yellow River course, explaining the formation of an impressive scarp and the more proximal location of the sediment source.

In addition to provenance analysis, grain size and shape characteristics obtained by dynamic image analysis (DIA) were used to fingerprint the transport processes of silt particles in a series of Quaternary loess-palaeosol sequences. The results revealed a decrease in the aspect ratio of the particles as a function of increasing grain size, thus indicating that systematic shape sorting occurred during the aeolian transport of the silt particles. A similar particle-shape sorting trend has also been found in a series of Red Clay

sequences, confirming that the Red Clay deposits are predominantly of aeolian origin. This study indicates that DIA of grain size and shape characteristics can be an additional powerful tool for fingerprinting trends in grain size and shape sorting, determining the dominant mode of transport, and reconstructing the transportation pathways of silt-sized aeolian sediments.

The final part of this thesis research comprised a pilot study on the use of the trace-element composition of quartz as a provenance tool to constrain the source area of the late Neogene and Quaternary dust deposits in Northern China. It revealed that quartz in the Mangshan loess deposits is largely derived from the Qaidam Basin of the NTP. The likely dust contribution from the Taklimakan Desert to the Red Clay deposits in Baode is also reflected in the trace element content of quartz. These results are comparable with the source signal obtained from the zircon U-Pb age spectra, suggesting that the trace element composition of quartz could be applied as an alternative tool to other single-grain provenance analytical approaches to track the dust source and dust pathways of the aeolian sediments.

Chinese abstract

摘 要

中国北方分布着世界上最厚，最为连续的风尘沉积-黄土和红粘土序列。这些沉积物蕴含着丰富的古环境变化信息。对于这些风尘物的物源变化研究不仅在于揭示它们的产生和搬运机制，更有助于我们理解晚新生代以来亚洲内陆风尘源区的干旱化过程以及大气环流格局的变迁。本论文通过分析中国黄土高原的黄土和红粘土剖面的沉积特征，综合使用传统和新型的沉积学和物源示踪方法来重建晚新近纪以来黄土高原风尘沉积物物源的时空变化及其传输路径，并探讨它们对于气候变化和构造演化的响应。

论文首先对黄土高原三个典型的晚中新世–上新世红粘土剖面（保德、蓝田以及董湾）进行物源的时空变化分析。本研究使用碎屑锆石的U-Pb年龄来约束沉积物的物源变化以及利用粒度端元模型（End member modelling）来分析红粘土的不同动力组分及其运移过程并结合回溯轨迹模型（backtrace trajectory modelling）来重建晚中新世的风尘传输路径。结果表明：青藏高原东北部（包括祁连山和柴达木盆地）的风化物是黄土高原西部（董湾）和南部（蓝田）风成红粘土的主要物源。此外塔克拉玛干沙漠的风尘输送也可能对董湾和蓝田红粘土中的细颗粒组分有所贡献。相反，黄土高原东北部的保德红粘土（保德组和静乐组），其风尘来源除了有来自青藏高原东北部的物质外，中亚造山带的风化物也是其组成成分。与黄土物源的研究对比发现，红粘土在物源上的空间异质性与第四纪黄土是一致的。我们还发现自3.6 Ma以来，静乐组红粘土中关于其西部物源区（青藏高原东北部和塔克拉玛干沙漠）的锆石年龄信号增加，表明更多物质从西部干旱区输送而来。这可能与上新世以来青藏高原以及天山的隆起所造成的西部干旱化加剧以及近地面的西风加强有关。此外，3.6 Ma 以来由于青藏高原的快速隆起，导致黄河从青藏高原向其冲积平原的物质输送增加，也可能是引起西部物源增加的原因。

为了进一步研究黄河对于中国北方第四纪风尘沉积的物质输送，我们选取了位于黄河下游的邙山塬的黄土–古土壤序列，对其沉积特征（粒度和沉积速率）和物源变化进行分析。邙山黄土剖面在古土壤层S2之上呈现出粗颗粒组分和沉积速率明显增加的趋势。以单颗粒锆石U-Pb年龄为依据的物源信号显示邙山黄土从黄土层L9沉积开始，其物源无明显变化；邙山黄土塬北部的黄河河漫滩是自黄土层L9沉积开始邙山风尘沉积物最主要的物源区。这暗示着黄河至少在L9沉积时已经贯穿三门峡，即黄河中游和下游贯通的时间应早于900 ka。邙山黄土–古土壤序列在古土壤层S2之上出现的剧烈的沉积特征的变化可能是由于渭河盆地在240 ka 发生的构造运动引起盆地北部河流下切，侵蚀加剧，造成更多的物质被输送到黄河下游所致。此外这一时期的构造运动可能导致黄河河道向南迁移，使黄河河漫滩更接近邙山塬，从而形成一个更近的物源区也是邙山S2以上粗颗粒组分增加的

原因。

论文第四章使用动态图像分析方法（dynamic image analysis，DIA ）对黄土高原黄土和红粘土沉积物的粒度和粒型进行分析并通过观察风尘沉积物中粉砂粒级的粒度–粒型的分布特征来研究其传输路径及运移过程。本研究发现黄土中粉砂粒级的颗粒物的长宽比随粒度的增加而减小，表明颗粒在风力运输过程中存在系统的形状分选。红粘土的粒度–粒型分布也呈现相同趋势，这意味着红粘土与黄土一样，均为风尘沉积物，其颗粒物的运移和黄土遵循同样的规律。

论文的最后一部分为使用碎屑石英中微量元素的含量来约束中国北方晚新近纪和第四纪风尘沉积物物源的初步研究。结果显示邙山黄土中石英颗粒的微量元素含量与青藏高原北部和柴达木盆地的碎屑物中的类似。此外，塔克拉玛干沙漠对保德红粘土的风尘贡献也反映在石英的微量元素含量上。这些结果与碎屑锆石U-Pb年龄所指征的物源信号具有可比性。本研究表明单颗粒石英中的微量元素含量可以作为风尘沉积物源区示踪的潜在研究方法。

Acknowledgements

This work started four years ago as a double doctorate program, carried out at the University of Helsinki in Finland and Vrije Universiteit Amsterdam, in the Netherlands. Accomplishing of this thesis in the two beautiful countries is a very unique and memorable experience for me. A great many people have offered their expertise and knowledge, support and inspiration over the course of this journey. Here, I would like to take this opportunity to express my sincere gratitude to them:

First and foremost, I am deeply indebted to my supervisor Dr. Anu Kaakinen. My PhD study would have never begun without Anu's kindly reply to my email in the spring of 2013. She introduced me to the world of research and provided me with the opportunity to work in a wonderful international project. It would be impossible to finish this PhD thesis without her constant support and contribution. I greatly appreciate the enormous time and patience she spent on mentoring me. She has always been positive and had faith in my work which significantly improved my confidence in doing research and motivated me to continue. Anu, words could never be enough to express my appreciation!

I was fortunate to work with other two brilliant supervisors Dr. Maarten A. Prins and Dr. Christiaan J. Beets in the Netherlands. I highly appreciate them for sharing their expertise, wisdom and time over the years. Their contribution and support during all the stages of this work has been of invaluable help. Many ideas were born during the inspiring discussions with them. I have been constantly impressed by their broad knowledge in the field and new perspectives in the research topic. Maarten and Kay, thanks for hosting me in VU and introducing me the colleagues there. Those "sightseeing tours" we had together in the Netherlands were really fun and a nice memory for me.

I am grateful to Prof. Mikael Fortelius in the University of Helsinki for his support and encouragement over the course of this project. Many thanks are owed to my VU promoter Prof. Ronald van Balen who was extremely helpful especially during the final stages of this work. I would like to thank the two pre-examiners Prof. Huayu Lu and Dr. Jan Berend Stuut for assessing the quality of this thesis and providing helpful comments.

I wish to thank all the co-authors for collaboration, for helping with fieldwork, laboratory analyses and their contribution at various stages of the manuscript. My special thanks are directed to Dr. Hui Tang and Dr. Tobias Fusswinkel for fruitful discussions and sharing their scientific expertise and skills.

I acknowledge the GeoDoc programme of the University of Helsinki for the financial support of several international conferences and other research visits abroad. I received the thesis completion grant from the University of Helsinki that enabled me to finalise this thesis. This work was supported by the funding of Academy of Finland.

I have had the joy and privilege of participating in the field work in Lantian and Mangshan. I wish to express my gratitude to Prof. Zhaoqun Zhang, Dr. Anu Kaakinen, Dr. Christiaan J. Beets and Dr. Bin Wang for help, sharing the adventure and inspiring discussions. I am grateful to all the colleagues involved in the earlier field investigations in Lantian, Baode, Dongwan and Mangshan. Their work has laid the foundation for my PhD thesis. I extend my gratitude to the colleagues of Beijing Normal University for their support.

I had great time in working at the Geological Survey of Finland (GTK) in Espoo where I

produced the extensive zircon U-Pb age dataset for my thesis. I want to thank the people there for their support and assistance. Especially, Dr. Yann Lahaye, Dr. Hugh O'Brien and Dr. Marja Lehtonen are highly appreciated for the time spending on my project and detailed guidance for the using of ICP-MS and SEM imaging and related data reduction.

I am much obliged to the colleagues and personnel in the Department of Geosciences and Geography, University of Helsinki who have made my work and life much easier and with a lot of fun. I send my gratitude to Prof. Tapani Rämö for his helpful suggestions in improving my first manuscript and for his interest in my project. I am grateful to Dr. Seija Kultti and Dr. Mia Kotilainen for their valuable advices and support related to my PhD study. I thank all the officemates (present and past) in C118: Outi Hyttinen, Leena Sukselainen, Paula Salminen, Bin Wang, and Joonas Wasiljeff for sharing the office and many joyful scientific and non-scientific conversations. I send my gratitude to Heikki Seppä, Juha Karhu, Tino Johansson, Helena Korkka, Aku Heinonen, Indrė Žliobaitė, Tuija Vaahtojärvi, Pasi Heikkilä, Mikko Haaramo, Hanna Reijola and Juhani Virkanen for various support and help. I would like to thank Marttiina Rantala, Mimmi Oksman, Ferhat Kaya, Yurui Zhang, Henrik Kalliomäki, Stefan Andersson, Radoslaw Michallik, Janina Rannikko, Liisa Ilvonen, Aleksis Karme, Normunds Stivrins, Peter Howett, Minja Seitsamo-Ryynänen and others for their friendship and vital peer support.

Benefited from this joint PhD project, I visited the Department of Earth Sciences, Vrije Universiteit Amsterdam quite often. I met many friendly and helpful people there and I wish to send my gratitude to them. In particular, I want to thank Roel van Elsas, chef of the mineral separation laboratory, for vital technical support and guidance. Roel is just capable of solving everything in the lab! Roel, thanks for taking me to the hospital when I accidently burned my arm. I want to thank Martine Hagen and Tineke Vogel-Eissens for assistance in grain size analysis and zircon separation. Tineke, it was a great experience to cycle with you in the beautiful countryside of Holland! My thanks also goes to Dr. Daniel Rits for helping me with many practical issues in VU.

Besides all my colleagues, I wish to thank my friends. My special thanks go to my badminton friends who have played the game with me weekly in Kumpula Unisport. I give my sincere gratitude to my Chinese friends in both Helsinki and Amsterdam. Thanks for sharing the delicious food, accompanying in holidays and events. All the activities we had together have enriched my life and enabled me to get rid of loneliness when studying abroad.

Last but not the least, I send my deepest gratitude to my family for their endless love and unconditional trust. I dedicate this thesis to them.

Contents

List of original publications

This thesis is based on the following publications:

I Shang, Y., Beets, C.J., Tang, H., Prins, M.A., Lahaye, Y., van Elsas, R., Sukselainen, L., Kaakinen, A., 2016. Variations in the provenance of the late Neogene Red Clay deposits in northern China. Earth and Planetary Science Letters 439, 88-100.

II Shang, Y., Prins, M.A., Beets, C.J., Kaakinen, A., Lahaye, Y., Dijkstra, N., Rits, D.S., Wang, B., Zheng, H.B., van Balen, R.T. Aeolian dust supply from the Yellow River floodplain to the Pleistocene loess deposits of the Mangshan Plateau, central China: evidence from zircon U-Pb age spectra. Quaternary Science Reviews. (in press)

III Shang, Y., Kaakinen, A., Beets, C.J., Prins, M.A., 2017. Aeolian silt transport processes as fingerprinted by dynamic image analysis of the grain size and shape characteristics of Chinese loess and Red Clay deposits. Sedimentary Geology, doi: 10.1016/j.sedgeo.2017.12.001. (in press)

IV Shang, Y., Kaakinen, A., Fusswinkel, T., Beets, C.J., Prins, M.A. Trace elements of detrital quartz as a provenance tool for Red Clay and loess in northern China. (in submission to Aeolian Research)

The publications are referred to in the text by their roman numerals.

Authors' contribution to the publications

Paper I

The study was designed by AK, CJB, HT, MAP and YS. YS conducted the zircon U-Pb analysis with aids of YL. HT conducted the dust trajectory modelling and provided the related text. MAP conducted the end member modelling of the grain size dataset. AK and LS analysed the grain size. The results were jointly interpreted by YS, AK, HT, CJB and MAP. YS prepared the manuscript with contributions from the other coauthors.

Paper II

The study was designed by MAP, CJB, AK and YS. YS conducted the zircon U-Pb age analysis with aids of YL; MAP conducted the end member modelling of the grain size dataset; ND, CJB and MAP conducted TGA and grain-size analyses. The results were jointly interpreted by YS, MAP, AK, CJB and RTvB. YS prepared the manuscript with contributions from the other coauthors.

Paper III
The study was designed by MAP, YS, CJB and AK. YS conducted the dynamic image analysis. MAP conducted the end member modelling of the grain size dataset. The results were jointly interpreted by YS and MAP. YS prepared the manuscript with contributions from the other coauthors.

Paper IV
The study was designed by AK, YS, MAP and CJB. The in situ quartz trace elements analysis was done by YS with aids of TF. The results were jointly interpreted by YS and AK. YS prepared the manuscript with contributions from the other coauthors.

Abbreviations

BD	Baode
BSE	Back-scattered electron images
CAOB	Central Asia Orogenic Belt
CLP	Chinese Loess Plateau
DIA	Dynamic Image Analysis
DJP	Duanjiapo
EMMA	End-member modelling algorithm
Fm	Formation
GAM	Gobi Altay Mountains
HX	Huanxian
ICP-MS	Inductively coupled plasma mass spectrometry
JL	Jingle
KDE	Kernel density estimation
LD	Laser diffraction
LT	Lantian
MDS	Multi-dimensional scaling
MLP	Mangshan Loess Plateau
MS	Mangshan
NCP	North China Plain
NTP	Northern Tibetan Plateau
PDP	Probability density plots
UH	University of Helsinki
VUA	Vrije Universiteit Amsterdam
XF	Xifeng
XY	Xunyi

List of tables and figures

1 Introduction

Airborne mineral dust generated from arid and semi-arid regions, once uplifted into the atmosphere, plays a significant role in the Earth system (Knippertz and Stuut, 2014). It interacts with climate by affecting the radiative budget, modifying atmospheric chemistry and contributing micronutrients to both terrestrial and marine ecosystems (Balkanski et al., 2007; Dentener et al., 1996; Schroedter-Homscheidt et al., 2013; Swap et al., 1992). In addition to the climate influence, dust and dust storms could also have severe environmental consequences along the transport pathways, such as affecting local air quality and impacting on human health by causing respiratory diseases and infections (Prospero et al., 2008). Dust records of the past, on the other hand, provide us with vital information on dust-related aspects of the Earth system over time, such as wind strength, atmospheric circulation patterns and variations in the vegetation cover. The Asian dry interior is regarded as one of the most important dust sources. Aeolian dust emitted from the Asian interior can be transported to proximal downwind regions such as the Chinese Loess Plateau (CLP) in northern China, and further eastwards over the Pacific Ocean and onwards onto the Greenland ice cap (Sugimoto et al., 2002; Sun et al., 2001). Notably thick and continuous dust deposits have accumulated in the CLP at least since the late Oligocene (Guo et al., 2002; Heller and Liu, 1982; Qiang et al., 2011). It has been suggested that the onset and formation of the aeolian deposits in the CLP have been affected by two remarkable processes during the Cenozoic: phased uplift of the Tibetan Plateau and Northern Hemisphere glaciation. In addition, both of these could have shaped the winds that transport the aeolian dust to the CLP (An et al., 2001). Deciphering such long terrestrial dust records would aid us in understanding the coupled effect of tectonic activity and regional climate on the changes in Earth surface processes during the Cenozoic. Knowledge of the dust provenance is the essential first step in exploring the whole dust pathway from source to sink. While contemporary dust sources can be recognised by means of Earth-orbiting satellites (Crusius et al., 2011; Muhs et al., 2014; Prospero et al., 2012), detecting the source areas of the palaeodust is not so straightforward.

Typically, dust records of the CLP are divided into three sequences: 1) Miocene loess (in the west of the Liupan Mountains) (Fig. 1), 2) Late Miocene-Pliocene Red Clay and 3) Quaternary loess-palaeosol (An et al., 2014; Guo et al., 2002; Liu, 1985). Loess is typically composed of silt-sized sediment particles and accumulated during glacial intervals when the Asian interior was colder and drier, while the palaeosols developed during interglacial periods when climate conditions were warmer and more humid. Red Clay is commonly regarded as a thick, fossiliferous, reddish soil complex primarily composed of clay and fine silt particles (Ding et al., 1998). While loess is considered to be of exclusively windblown origin, the bottom part of Red Clay deposits in some sites has been argued to be of fluvial origin or reworked by fluvial process (Alonso-Zarza et al., 2009; Guo et al., 2001; Nie et al., 2014; Zhang et al., 2013). Nevertheless, the main body of the Red Clay sequences has been well acknowledged as being of aeolian origin, based on field observations and grain-size, geochemical and magnetic property analysis (An et al., 2001, 2014; Ding et al., 1998; Ding et al., 2001a; Guo et al., 2001; Lu et al., 2001; Sun et al., 1997). Inferred from modern dust observations, dust on the CLP has been suggested to be generated from the arid Asia interior through transportation by near-

surface winds of the winter monsoon resulting from the Siberian–Mongolian high-pressure system and/or westerly jet (Ding, 2005; Roe, 2009). Following this regime, a large number of arid regions located west and north of the CLP that are capable of producing silts could be potential source areas for the CLP dust (Fig. 1). These arid regions are characterised by a range of landscapes, such as high mountains, gobi (stony desert) and sandy lands, fluvial fans, yardangs, playas and piedmonts (Pye, 1995; Pye and Zhou, 1989; Smalley et al., 2009; Sun et al., 2002).

The source, or sources, of the aeolian loess in the CLP have been disputed for decades. Previous studies based on grain-size records of the loess-palaeosol sequences have demonstrated that in the central CLP, the loess grain size shows an approximately north–south decreasing trend, particularly during glacial intervals. Systematic decreases in the loess thickness have been observed along the same transect as a consequence of sediment load reduction in a downwind direction (Ding et al., 2002; Nugteren and Vandenberghe, 2004; Prins and Vriend, 2007; Pye, 1995). These observations suggest a dominant north–south dust transport pathway for loess deposits in the CLP and the presence of a proximal dust source or sources north and northwest of the CLP. Based on isotopic, geochemical and mineralogical analyses, Sun (2002) proposed that the gobi in southern Mongolia and the adjacent gobi and sandy deserts of northern and northwest China (the Badain Jaran, Tengger, Ulan Buh, Hubq and Mu Us Deserts) are the main source areas

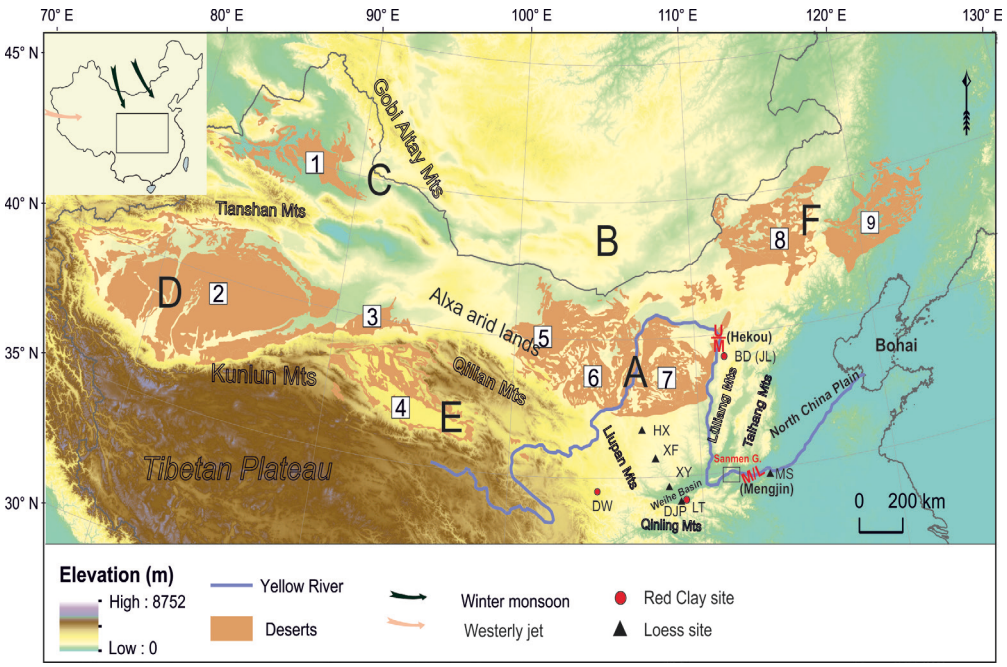

Figure 1. Map of Northern China. Numbers 1–9 indicate the major deserts in western, northern and eastern parts of the CLP. 1 - Gurbantunggut (Jungger Basin), 2 - Taklimakan (Tarim Basin), 3 - Kumtag, 4 - Qaidam, 5 - Badain Jaran, 6 - Tengger, 7 - Mu Us, 8 - Otindag and 9 - Horqin. The black triangles mark the loess section, while the red dots indicate the Red Clay sites of this study. HX - Huanxian, XF - Xifeng, XY - Xunyi, DJP - Duanjiapo, MS - Mangshan, DW - Dongwan, LT - Lantian, BD - Baode and JL - Jingle. A–F indicate the grouped potential source areas for the CLP. A - adjacent deserts north and northwest of the CLP; B - southern Mongolia Desert; C - Jungger Basin and Gobi Altay Mountains; D - Taklimakan Desert; E - Northern Tibetan Plateau, including Qilian Mountains and Qaidam Basin; F - deserts northeast of the CLP. The red letters indicate the boundaries of the upper and middle reaches and the middle and lower reaches of the Yellow River.

for the CLP loess, rather than the three inland basins: the Tarim, Qaidam and Jungger Basins (Fig. 1). However, Sun (2002) pointed out that those deserts actually acted as the source holding areas rather than the dust producers. According to Sun (2002), silts in the CLP dust records are ultimately produced from high mountain ranges ("High Asia") such as the Gobi Altay Mountains (GAM) and Qilian Mountains during "mountain processes" (i.e. glacial grinding, tectonic processes, frost weathering, salt weathering and fluvial comminution). The provenance signal inferred from radiogenic isotope data ($^{87}Sr/^{86}Sr$ and $^{143}Nd/^{144}Nd$) suggests that the "western deserts", the deserts and arid lands located west of the CLP (Qaidam Basin, Badain Jaran Desert and Tengger Desert), rather than the "northern deserts" (Hobq Desert and Mu Us Desert), were the main source regions for the CLP dust during glacial stages (Chen et al., 2007). A recent study based on the same methods also pointed out a constant dust supply to the CLP from the region between the Qilian Mountains and GAM, i.e. the Alxa arid lands, since the early Miocene (Chen and Li, 2013).

In recent years, the application of single-grain zircon U-Pb dating techniques has allowed the discrimination of multiple potential source areas for the CLP dust. The advantage of single-grain analysis in provenance studies over bulk analysis techniques is that it will not average out signatures from multiple source areas. Zircon U-Pb chronology has revealed a significant dust supply from the northern and northeastern Tibetan Plateau and Qaidam Basin, mixed with additional contributions from the GAM and northern China Craton to the CLP loess deposits (Bird et al., 2015; Che and Li, 2013; Licht et al., 2016a; Pullen et al., 2011; Stevens et al., 2013; Zhang et al., 2016). Moreover, the zircon U-Pb age spectra also indicate spatial variation in the dust source of the loess deposits across the CLP (Bird et al., 2015), although whether there are any temporal (e.g. glacial/interglacial) variations in the provenance of loess-palaeosol sequences remains uncertain and debated (Bird et al., 2015; Che and Li, 2013; Licht et al., 2016a; Xiao et al., 2012).

What is still ambiguous is how the sediments were transported from the source area(s) to the CLP. Some studies have advocated direct transport from the north and northwest by winds passing over the Mu Us Desert, Tengger Desert and Badain Jaran Desert during interglacial stages, and from the west through the Qaidam Basin and Qilian Mountains during glacial stages (Kapp et al., 2011; Pullen et al., 2011). However, inferred from the results of mixing modelling on the loess grain-size dataset, Prins et al. (2007) and Prins and Vriend (2007) suggested the opposite pattern. Others have addressed the significant contribution of Yellow River sediments to the CLP dust based on the zircon age provenance data. They have interpreted that the sediments were first carried by the Yellow River from the Northern Tibetan Plateau (NTP) to the floodplain northwest of the Mu Us Desert (Yinchuan-Hetao Graben), and were then entrained by near-surface winds to the downwind CLP (Nie et al., 2015; Stevens et al., 2013). Studies on the sedimentology of a loess-palaeosol sequence in the Mangshan Loess Plateau (MLP) in the lower reach of the Yellow River indicate that the Yellow River floodplain has been the main dust source of the aeolian loess deposits in the southeastern part of the CLP during the last glacial-interglacial cycle (Prins et al., 2009; Zheng et al., 2007). However, no diagnostic provenance evidence is currently available for this. The MLP is located just downwind of the Yellow River floodplain and near the boundary of the middle and lower reaches of the Yellow River (Fig. 1). Reconstruction of the dust supply history of the

loess-palaeosol sequence in the MLP would provide a case study to examine the role of the Yellow River in transporting sediments to the aeolian deposits in the CLP and further help us to understand the developmental history of the drainage system of the Yellow River.

While numerous studies have focused on the provenance analysis of Quaternary loess-palaeosol sequences, the sediment source(s) for the late Neogene Red Clay deposits are less well studied and understood. Nie et al. (2014) provided the first provenance data based on the zircon U-Pb age components for the Red Clay sequence in the central CLP, and their results revealed multiple sources for these deposits: dust generated from the Taklimakan Desert by westerly winds is the dominant source for the early Pliocene Red Clay, whereas late Pliocene Red Clay is similar to the source of the Quaternary loess, and was mainly derived from the NTP. However, it is still unclear whether the source, or sources, of the Red Clay is spatially variable due to a paucity of available provenance data. Detailed and systematic provenance work on multiple Red Clay sites across the CLP was needed to better constrain the source areas and the transport pathways of the Red Clay and thus the wind patterns responsible for dust delivery during the Late Neogene.

2 Study area, studied sites and collected material

2.1 Chinese Loess Plateau

The Chinese Loess Plateau (CLP), with an elevation varying between 800 and 3000 metres, extends from 32°N to 40°N and from 98°E to 115°E, covering about 600,000 km^2 in northern China (Liu, 1999). It largely overlaps with the upper and middle reaches of the Yellow River drainage area and is bounded by the Mu Us Desert to the north, the Qinling Mountains to the south, the Helan Mountains to the northwest, the Qilian Mountains to the west and the Taihang Mountains to the east (Fig. 2). The climate in this area is highly seasonal and monsoon influenced: in winter, the stable Siberian-Mongolia anticyclone results in a cold and dry air flow coming from the north and the northwest known as the East Asian winter monsoon, while in summer, moisture is brought to the continent by the warm air flow from the ocean in the south and southeast, known as the East Asian summer monsoon. The mean annual temperature in the region increases from from 4 °C in the northern CLP to 14 °C the southern CLP, and the mean annual precipitation rises from less than 200 mm in the northwest to 650 mm in the southeastern CLP (UCAR, 2006). Along this climatic gradient, the modern vegetation cover changes from arid steppe to forest steppe and finally to broadleaved forest in a southeastern direction.

The CLP is famous for its characteristic loess landscapes and continuous Neogene and Quaternary dust records. According to the tectonic setting and loess landscapes, the CLP can be grouped into three regions (Fig. 2): I) the Ordos Block, II) the Longzhong Basin and III) the Fenwei Graben (Yuan et al., 2012).

The central CLP lies within the body of the Ordos Block. The Ordos block is rimmed by the Hetao Basin to the north, the Liupan Mountains to the west, the Weihe Basin to the south and the Lüliang Mountains to the east. During the early Cenozoic there was tectonic quiescence; the area suffered extensive erosion, which resulted in the formation of a gentle-sloped planation surface (Nie et al., 2016; Yuan et al., 2012). During the late Cenozoic, due to the India–Asian collision and uplift of the Liupan Mountains, the planation surface was disrupted and the area was dissected into a maze of gullies and hills. Three main loess landform types are distinguished in the area:

plateau or tableland (called Yuan in Chinese), elongated ridges (Liang) and hemispherical hills (Mao) (Liu, 1985). The most complete Neogene-Quaternary aeolian records are found within this region, where the Quaternary loess deposits conformably overlie the late Miocene-Pliocene Red Clay. The continuous loess-palaeosol sequences found in the central CLP consist of 33 palaeosol and 34 loess units with a depositional age spanning from ~2.6 to 0 Ma (Liu et al., 1999). Most Red Clay sequences in the Ordos Block have a basal age of ~7–8 Ma (Ding et al., 2001b; Qiang et al., 2005; Sun et al., 1998).

The Longzhong Basin is located west of the Liupan Mountains and its western and southwestern borders extend to the NTP. It is a Cenozoic foreland basin resulting from the India–Asian collision (Horton et al., 2004). This region is characterised by the Red Clay landform of Neogene age, covered with a thin loess layer. Exceptionally thick loess successions of up to 300 m are found in the Lanzhou area (An et al., 2001; Liu, 1985; Yuan et al., 2012). Aeolian dust deposition in this region started at least 22 Ma (Guo et al., 2001); a recent study extended the basal age of the sequence back as far as to 25 Ma (Qiang et al., 2011).

The Fenwei Graben of the eastern CLP is a crescent-shaped rift valley bordered by the Ordos Block to the west, the Qinling Mountains to the south and the Taihang Mountains to the east. It is comprised of two sub-basins: the Weihe Basin in the southwest and the Fenhe Basin in the north and northeast, covering an area of more than 20,000 km^2. This graben experienced continuous subsidence during the Eocene due to the eastward extrusion of the Tibetan Plateau and has been filled by remarkably thick deposits (AFSOM, 1988; Hu et al., 2016; Liu et al., 1960; Rits et al., 2017; Zhang et al., 1978). Thick lacustrine sediments indicate that there was a large palaeolake (Sanmen Lake) in the Weihe Basin extending from the Sanmen Gorge westwards to Baoji (AFSOM, 1988; Kong et al., 2014). It has been suggested that the lake was drained due to the incision of the Yellow River through the Sanmen Gorge (Kong et al., 2014;

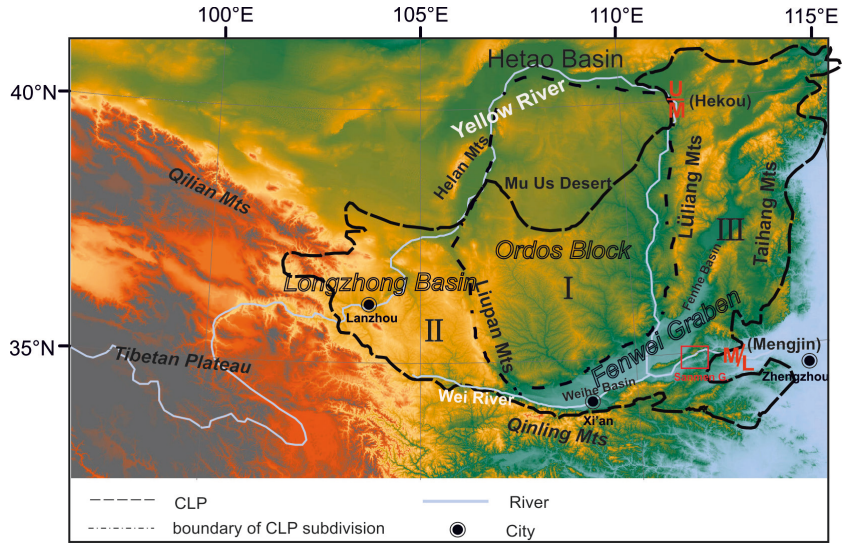

Figure 2. The Chinese Loess Plateau and three subdivisions: I, the Ordos Block; II, the Longzhong Basin and III, the Fenwei Graben. The red letters indicate the boundaries between the upper and middle, and the middle and lower reaches of the Yellow River. The red rectangle marks the location of the Sanmen Gorge. The figure is modified after Yuan et al. (2012).

Wang, 2002; Yuan et al., 2012). In the Fenwei Graben, Quaternary loess deposits overlie the lacustrine sediments or river terraces, forming the yuan tableland loess landscape. Here, Red Clay sequences are sporadically found. Two typical and well-studied Red Clay sites are the Lantian site in the southwest corner of the Weihe Basin (Kaakinen and Lunkka, 2003; Zhang et al., 2013) and the Yushe site on the eastern flank of the Lüliang Mountains (Flynn and Wu, 2017; Flynn et al., 2011; Tedford et al., 2013).

2.2 Yellow River

With a total length of 5500 km, the Yellow River (Huanghe) is one of the largest rivers of the world. It originates from the northern Tibetan Plateau and has deeply incised into a series of intermontane basins and bedrock ranges along the northeastern plateau margin. After a 1500-km-long U-bend developed around the Ordos Block, it runs through the Sanmen Gorge and flows onto a wide floodplain in the low-gradient eastern part of China (North China Plain, NCP) and eventually discharges into the Bohai Sea (Fig. 1). Traditionally, the river has been divided into an upper, a middle and a lower reach. The boundary between the upper and middle reaches is located near Hekou town on the northeastern edge of the Ordos Block, while transition between the middle and lower reaches is located at Mengjin near the Mangshan Loess Plateau. Since the Yellow River flows through the CLP, which is subject to high erosion rates, it is currently one of the most sediment-laden rivers in the world. It has been proposed that the integration of the modern Yellow River is a consequence of cutting through of a series of isolated inland fluvial-lacustrine basins by headward erosion (Craddock et al., 2010). However, the geological history of the Yellow River, particularly for its middle and lower reaches, is still largely debated, and the suggested timing for the full incision of the Yellow River through the Sanmen Gorge varies from the Late Miocene to the Pleistocene (Craddock et al., 2010; Hu et al., 2017; Kong et al., 2014; Lin et al., 2001; Wang, 2002; Wang et al., 2013).

2.3 Red Clay sites

In this study, three Red Clay sites (Baode, Lantian and Dongwan; see Figure 3, Figure 4 and Table 1) representing a variety of geographical and local sedimentary settings across the CLP were investigated.

The Baode site in the northeastern CLP is surrounded by the Lüliang Mountains to the east and the Yellow River to the west (Fig. 1). Baode is an area where the "*Hipparion* fauna" in northern China was discovered, and the term "*Hipparion* Red Clay" was then established by Zdansky (1923) to define the fossiliferous Red Clay deposits in the area. The late Neogene Red Clay and Quaternary loess-palaeosol strata are exposed in steeply sloping gullies and ravines and rest on the Palaeozoic basement with an angular unconformity. The late Neogene stratigraphy of Baode has been grouped into two formations: the Baode and Jingle Formation (Fm) (Kaakinen et al., 2013; Teilhard de Chardin and Young, 1931; Zhu et al., 2008). The underlying Baode Fm is typically about 60 m thick and contains abundant mammalian fossils of the late Miocene age. It has a more variable lithology compared to the overlying Jingle Fm. The lower part of the Baode Fm has abundant conglomerates of varying thickness, whilst the upper part, representing the bulk of the Baode Fm, is composed of red brown clays and silts with alternating carbonate nodule-rich horizons and infrequent sheet conglomerate beds. The Jingle Fm is up to ca. 40 m thick and conformably overlies the Baode Fm. It is exclusively composed of clay and silt-sized lithologies with a distinctive deep red colour

and is devoid of sand and gravel lithologies. Carbonate-rich horizons and abundant Fe-Mn coating present in the deposits indicate strong pedogenesis of the soil. Magnetostratigraphic dating has assigned a basal age of 7.23 Ma to the Baode Fm and a depositional age of 5.23 to 2.72 Ma to the Jingle Fm (Kaakinen et al., 2013; Zhu et al., 2008).

The Lantian site in the southernmost CLP is located in the foothills of the northern flank of the Qinling Mountains, within the southeastern Weihe Basin. It is comprised of a thick accumulation of Cenozoic clastic sediments (Kaakinen, 2005). The late Neogene sediments in this area include the Lantian Fm and the underlying Bahe Fm. With a thickness of 280 m, the Bahe Fm is mainly composed of fluvial deposits characterised by thick and laterally continuous floodplain deposits (Kaakinen and Lunkka, 2003; Zhang et al., 2013). Based on geochemical and grain-size evidence, these fine-grained units have been suggested to be partly aeolian (Wang et al., 2014). The overlying the Lantian Fm is a Red Clay succession comprising distinctive deep-red fine-grained deposits with cyclic carbonate nodule-rich horizons progressively becoming more abundant in the upper part of the formation (Figs. 4c and 4d). As demonstrated by magnetostratigraphic dating studies (Kaakinen, 2005; Wang et al., 2014; Zhang et al., 2013), the basal age for the Bahe Fm is at ca. 11 Ma and the boundary between the Bahe and Lantian Fm is ca. 7 Ma.

The Dongwan Red Clay succession in the western CLP represents the loessic Red Clay

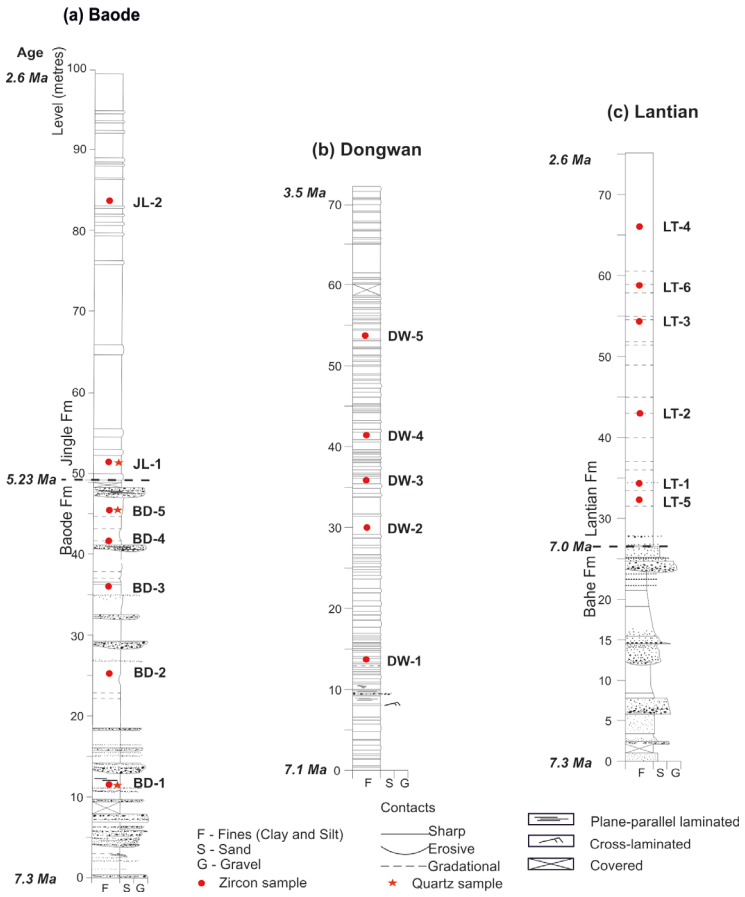

Figure 3. Lithology of the studied Red Clay sites (a) Baode (Jingle), (b) Dongwan and (c) Lantian. Red dots and red stars mark the levels of samples collected for zircon U-Pb dating and in situ quartz trace element analysis, respectively. The samples for dynamic image analysis of grain size and shape are not marked here, but are shown in Fig. S1 in Paper III.

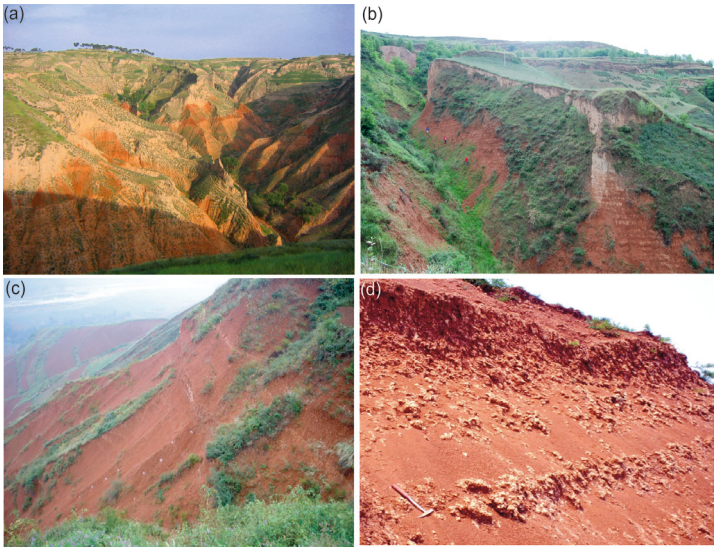

Figure 4. The studied Red Clay sites of (a) Baode, (b) Dongwan and (c) Lantian and (d) the carbonate nodule-rich horizon of the Lantian Fm. Photos by Anu Kaakinen.

deposits in the west of the Liupan Mountains (Fig. 1). It is characterised by a 74-m-thick sequence of dominantly massive reddish silt beds and carbonate rich couplets, with thin laminations indicating water-lain settling recognized in the lower part of the sequence (Fig. 3). Fossil micromammals (Liu et al., 2011, 2013) and terrestrial molluscs (Li et al., 2014) are present throughout the sequence. Compared to the Red Clays of Baode and Lantian, relatively weaker nodule formation is shown in the carbonate units in Dongwan. According to Hao and Guo (2004), the Dongwan Red Clay succession is dated to the time interval of 7.1 to 3.52 Ma based on magnetostratigraphy.

Samples were taken from the fine-grained lithologies. For the Baode Fm and lower part of the Lantian Fm, where conglomerates or sandstones are shown, laterally equivalent fine-grained facies was sampled, when possible. The sampling level for zircon U-Pb age dating and for analysis of the trace element content in quartz is indicated in Figure 3.

2.4 Loess-palaeosol sequences

To characterise the transport pathways of loess across the central CLP, four loess-palaeosol sections located along a transect oriented north-to-south across the main body of the CLP, Huanxian (HX), Xifeng (XF), Xunyi (XY) and Duanjiapo (DJP), were selected and sampled for grain size and shape analysis (Fig. 1). Detailed descriptions and age models of the sections are presented in Nugteren and Vandenberghe (2004) and Prins and Vriend (2007). All the sections cover the last two glacial and interglacial cycles (S0–L1–S1–L2–S2), except the DJP sequence in the southernmost CLP, which comprises the last glacial–interglacial period (S0-L1) (Fig. 5). Samples from the same stratigraphic intervals representative for the typical loess (glacial and stadial loess L1-1, L1-3, L2-1 and L2-3), well-developed soil (interglacial palaeosol, S1 and S2) and poorly developed soil (interstadial palaeosol, L1-2 and L2-2) units of individual loess sections were collected (Fig. 5a–5d).

In this work (Paper II), a detailed study of the sedimentology and provenance of the loess-palaeosol sequence from the Mangshan Loess Plateau (MLP) was carried out. Mangshan is

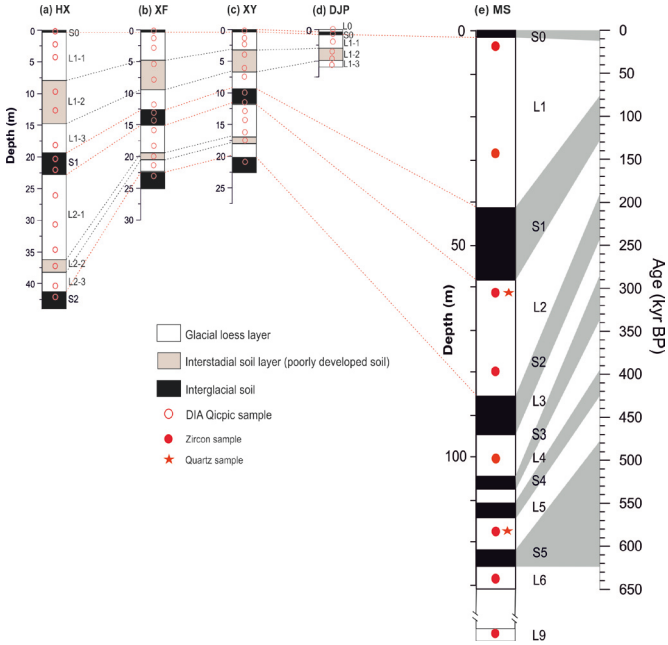

Figure 5. Stratigraphy of the studied loess sections: (a) HX - Huanxian, (b) XF - Xifeng, (c) XY - Xunyi, (d) DJP - Duanjiapo and (e) MS - Mangshan. DIA - dynamic image analysis. The age model for the Mangshan section was established by correlating the loess proxy records with the oxygen-isotope composite record from Donghu, Sanbao and Hulu caves in central China (Wang et al., 2008; Cheng et al., 2009, 2016). For a detailed description of the age model, see Paper II.

located near the boundary of the middle and lower reaches of the Yellow River (Fig. 1), and in the topographic transition border between the uplifting region in the west and subsiding region in the east. About 200 km upstream, the Yellow River cuts through the Sanmen Gorge, initially releasing a tremendous silt load from the CLP. This results in the formation of a large fluvial-alluvial fan east of the gorge, which constitutes the southwestern part of the NCP. Downstream, the Yellow River gradually flows through the NCP with a low gradient and eventually discharges into the Bohai Sea. Typical loess-palaeosol successions are well exposed on the northern slope of the MLP, where the Yellow River has laterally cut the plateau and formed a deep scarp along its northern edge (Fig. 6). Field observations have identified 11 loess units and 12 palaeosol units for the exposed Mangshan loess deposits (Ji et al., 2004; Qiu and Zhou, 2015; Zheng et al., 2007). The studied section of this work, with a total thickness of 171 m, is located near the village of Liugou, about 25 km northwest of Zhengzhou city. The magnetostratigraphy has been established by Zheng et al. (2007), setting the Brunhes/Matuyama (B/M) boundary at a depth of about 150 m in the lower part of loess unit L8 in the section, demonstrating the resemblance between the Mangshan loess sequence and the other typical loess-palaeosol sequences found on the CLP. The upper part of the sequence (upper 100 m, above palaeosol S2) (Fig. 5) is characterised by higher sedimentation rates and coarser-grained loess sediments compared to the lower part of the sequence and the loess deposits in the central CLP (Prins et al., 2009; Qiu and Zhou, 2015; Zhang et al., 2004; Zheng et al.,

Figure 6. Mangshan Loess Plateau (MLP) in the lower reach of the Yellow River. Photo by Yuan Shang.

2007). In this study, the main focus was on the upper 130 m of the Mangshan Plateau sequence, which covers palaeosol unit S0 to loess unit L6, with an additional (zircon) sample taken from loess unit L9.

3 Objectives of the study

The main aim of this (PhD) study was to provide a comprehensive approach to examine the long-term dust supply and transport patterns developing during the late Neogene and Quaternary in the CLP of northern China, and their response to changes in climate and tectonic evolution. To this end, a combination of both conventional and novel sedimentological and provenance analytical methods was used.

The specific objectives were:

1) To provide a detailed provenance analysis based on the zircon U-Pb ages for the late Miocene-Pliocene Red Clay sequences to investigate the spatial and temporal variations in the sources of the Red Clay, and to subsequently investigate the dust transport pathways and prevailing wind patterns during the late Neogene by dust trajectory modelling (Paper I);

2) To investigate the role of the Yellow River in supplying dust to the Quaternary loess deposits and study the mechanisms that control the sedimentology and provenance changes of the loess-palaeosol sequences (Paper II);

3) To examine the subpopulations and their relative proportions in the bulk Red Clay and loess deposits by applying an end-member modelling approach to an extensive grain-size dataset. The aims were to understand the dust transport process related to each subpopulation and examine the (dis-)similarity of the transport and depositional processes between Red Clay and loess deposits (Papers I and II);

4) To determine the dust transport pathways and reveal the aeolian sorting pattern by applying dynamic image analysis (DIA) to characterise the grain size and shape distribution of the silt and fine sandy particles of the loess and Red Clay deposits (Paper III);

5) Test the application of the trace element content in quartz grains as an alternative tool to determine the dust source of the aeolian loess and Red Clay deposits (Paper IV).

4 Methods

The analysis conducted for each of the studied sites is summarised in Table 1.

4.1 Grain size and shape analysis

Grain-size analysis was performed for Red Clay and loess samples in Papers I, II and III. Following the standard analytical procedure for loess and Red Clay (cf. Konert and Vandenberghe, 1997; Vandenberghe et al., 2004), about 0.5–1 g of bulk sediment was pre-treated with H_2O_2 and HCl to remove organic matter and carbonates, respectively. The grain-size records of the loess sections Huanxian, Xifeng, Xunyi, Duanjiapo and Mangshan, and of the Red Clay section of Lantian were obtained using a Fritsch A22 laser diffraction (LD) instrument at Vrije Universiteit Amsterdam (VUA). Red clay samples from the Jingle Fm of Baode and from Dongwan were analysed using a Sympatecs KR laser diffraction particle sizer at VUA. Red Clay samples of the Baode Fm were analysed using a Coulter LS200 at the University of Helsinki (UH). All the LD devices used in this study produce grain-size distributions with 56 size intervals within the size range 0.15–2000 μm. We used the GRADISTAT program developed by (Blott and Pye, 2001) to calculate the median grain sizes of the samples.

The image analysis sensor Qicpic/R (http://www.sympatec.com/EN/ImageAnalysis/

Table 1. Description of the studied Red Clay and loess sections and related methods.

Sites	Late Miocene-Pliocene Red Clay			Quaternary loess				
	Baode (Jingle)	**Lantian**	**Dongwan**	**Mangshan**	**Huanxian**	**Xifeng**	**Xunyi**	**Duanjiapo**
Coordinates	38.99°N 111.14°E	34.25°N 109.12°E	34.96°N 105.78°E	34.95°N 113.37° E	36.6°N 107.3°E	35.88°N 107.97°E	35.06°N 108.3°E	34.2°N 109.4°E
Studied age interval	7.23 – 3.5 Ma	5.83 – 3.7 Ma	6.73 – 4.36 Ma	900 ka – 0 (L9–S0)	225 ka – 0 (S2–S0)	225 ka – 0 (S2–S0)	225 ka – 0 (S2–S0)	70 ka – 0 (L1–S0)
Sample analysis	Grain size (LD, DIA) Grain shape (DIA) Zircon U-Pb Quartz trace elements	Grain size (LD, DIA) Grain shape (DIA) Zircon U-Pb	Grain size (LD, DIA) Grain shape (DIA) Zircon U-Pb	Grain size (LD) Zircon U-Pb Quartz trace elements Carbonate content Organic content	Grain size (LD, DIA) Grain shape (DIA)	Grain size (LD, DIA) Grain shape (DIA)	Grain size (LD, DIA) Grain shape (DIA)	Grain size (LD, DIA) Grain shape (DIA)
Statistical analysis	EMMA MDS	EMMA MDS	EMMA MDS	EMMA MDS	EMMA	EMMA	EMMA	EMMA
Climate modelling	Dust trajectory modelling	Dust trajectory modelling	Dust trajectory modelling					
Paper	I, III, IV	I, III	I, III	II, IV	III	III	III	III

QICPIC.html) developed by Sympatec was used in Paper III to characterise the grain size and shape of silt and fine sandy particles in the loess and Red Clay deposits. This was the first time that dynamic image analysis (DIA) had been applied to Chinese aeolian dust. The pre-treatment of the Red Clay and loess samples for DIA followed the same procedure as the LD grain-size analysis to ensure that the particles were well dispersed during measurement. DIA provides information of the size and shape of a particle based on a 2D image of the particle's contour. In this study, the mean Feret diameter and aspect ratio were used to describe the size and shape of a particle, respectively. Additionally, silty and sandy size fractions expressed as parts per million (ppm) of the total number of particles analysed (bulk sample) were calculated for the Red Clay and loess samples in order to investigate the grain-size components of bulk sediments. The particle counts of the >32 μm, >63 μm, >125 μm and >250 μm fractions were reported and included for detailed analysis.

4.2 Zircon U-Pb dating

Detrital zircon U-Pb dating was used to characterise the provenance of the Red Clay and loess deposits in Papers I and II. Separation of the zircon grains from the bulk samples was conducted at the Mineral Separation Laboratory of VUA. About 0.5–5 kg of bulk sediments was wet-sieved over a 20-micron sieve and treated with 5% HCl to remove carbonate. Zircon grains were collected after heavy liquid (density of 2.86 and 3.30 g/cm^3 LST heavy liquid) and Frantz magnetic separation. Zircon grains were handpicked and mounted in a 2.5-cm-diameter epoxy resin disc, sectioned approximately in half and polished. In addition, photomicrographs of zircons were taken with an Olympus stereo zoom microscope for zircon morphology analysis before mounting and polishing. Back-

scattered electron images (BSE) were prepared for the zircons to target the spot sites.

Detrital zircon U-Pb ages were determined by laser-ablation inductively coupled plasma mass spectrometry (ICP-MS) at the Finnish Geosciences Research Laboratory, Geological Survey of Finland, in Espoo. Red Clay samples of Lantian, Dongwan and Baode were analysed with a Photon Machine Analyte G2 laser microprobe using a similar technique as in (Rosa et al., 2009). The loess samples and fluvial samples were analysed by a Nu Plasma AttoM single collector ICPMS connected to a Photon Machine Excite laser ablation system. Typical ablation conditions included a beam diameter of 20–29 μm, a pulse frequency 5 Hz and a beam energy density of 2 J/cm^2. The calibration standard GJ-1 (609 ± 1 Ma) (Belousova, 2005) and in-house standards A382 (1877 ± 2 Ma) and A1772 (2712 ± 1 Ma) (Huhma et al., 2012) were run at the beginning and end of each analytical session, and at regular intervals during sessions. The Glitter program was used for calibration of the raw data (Van Achterbergh et al., 2001). All the ages were calculated with 2σ errors and without decay constants errors. The $^{207}Pb/^{206}Pb$ age offset from concordant ID-TIMS ages for several samples did not exceed 0.5%. We used $^{238}U/^{206}Pb$ ages for ages younger than 1 Ga and $^{207}Pb/^{206}Pb$ ages for ages older than 1 Ga. Ages were rejected if discordance exceeded ±15% for Red Clay and ±10% for loess and fluvial sands.

4.3 Trace element content in quartz

In the study presented in Paper IV, we explored the possibility of using the trace element content in quartz as a provenance tool for the loess and Red Clay deposits. The preparation work required thorough cleaning of the quartz grains in order to remove clay minerals and other potential contamination attached to the surface of the quartz. The trace element concentration in quartz was measured with an Agilent 7900s ICP mass spectrometer coupled with a Coherent GeoLas Pro MV 193 nm excimer laser-ablation system at the Department of Geosciences and Geography, University of Helsinki. The detailed set-up for the measurement is presented in Paper IV. The instrument accuracies of 39 elements were monitored daily by measuring the composition of NISTSRM612 synthetic glass standards using NISTSRM610 as the external standard. The measurements were accepted if the concentrations were within 5% of the preferred values and the propagated uncertainties associated with NISTSRM610 and NISTSRM612 (Spandler et al., 2011). The following trace elements were included in the mass scan table: ^{7}Li, ^{11}B, ^{23}Na, Mg^{25}, ^{27}Al, ^{31}P, ^{34}S, ^{35}Cl, ^{39}K, ^{42}Ca, ^{45}Sc, ^{47}Ti, ^{49}Ti, ^{55}Mn, ^{57}Fe, ^{65}Cu, ^{66}Zn, ^{71}Ga, ^{72}Ge, ^{85}Rb, ^{88}Sr, ^{90}Zr, ^{133}Cs, ^{137}Ba, ^{208}Pb and ^{238}U. However, only ^{7}Li, ^{45}Sc and ^{49}Ti were found to consistently be suitable for application as provenance tracers. The energy density was 10 J/cm² for the standard NISTSRM610 and 14 J/cm² for quartz. For each analysis, the repetition rate was 10 Hz and the dwell time per isotope was 10 ms. Laser spot sizes from 30~90 μm were used, depending on the grain size of the quartz.

4.4 End-member modelling of grain-size distributions

Sediment fluxes from multiple sources and transporting patterns can be detected by means of end-member modelling of the grain-size distribution (Stuut et al., 2002; Weltje and Prins, 2003, 2007). This has been well used in distinguishing aeolian from fluvial input in various marine settings (Deplazes et al., 2014; Prins et al., 2000; Stuut et al., 2002, 2014). Previous studies have also suggested that a genetically meaningful unmixing of loess grain-size distributions can be accomplished with an

end-member modelling algorithm (EMMA) (Prins and Vriend, 2007; Prins et al., 2009; Vriend and Prins, 2005; Vriend et al., 2011). In this work, we applied the EMMA to the grain-size distributions of both the Quaternary loess-palaeosol sequences (Paper II and III) and late Miocene-Pliocene Red Clay sequences (Paper I and III) to characterise the subpopulations of the mixed aeolian sediments (and their relative contribution within the sections) and to distinguish the possible fluvial input in the Red Clay deposits.

End-member modelling consists of two stages: in the first stage, the numbers of end members (EMs) are estimated according to the mean coefficient of determination (r^2), and in the second stage, the proportions of each EM are calculated. The coefficient of determination (r^2) represents the proportion of the variance of each grain size reproduced by the approximated data (Weltje, 1997). The mixing model is chosen when the r^2 shows a satisfactory goodness of fit (usually >0.8). This means that the selected model provides a good description of the variation in the grain-size distribution dataset.

4.5 Visualisation of zircon U-Pb data and the multi-dimensional scaling (MDS) map

Probability density plots (PDP; Ludwig, 2003), kernel density estimation (KDE, Vermeesch, 2012) plots and histogram diagrams were used to visualise the zircon age distributions of Red Clay and loess samples. Zircon grains from different stratigraphic units are combined within the section in order to better assess the difference between individual sites and to reduce the bias and statistical errors brought about by (too) small sample sizes. A non-metric multi-dimensional scaling (MDS) map (Vermeesch, 2013) was employed to visualise the (dis)similarities between the combined large zircon datasets of Red Clay, loess and the sediments of potential source areas. This technique works in a similar way to principal component analysis, which is able to capture the main feature of the detrital zircon age datasets and has been well practiced in previous provenance studies on Red Clay and loess (Bird et al., 2015; Che and Li, 2013; Nie et al., 2014; Stevens et al., 2013; Vermeesch, 2013). We also used the MDS map for visualising a comparison of trace element contents in quartz from the Red Clay, loess and desert sands samples.

4.6 Dust trajectory modelling

The trajectory model HYSPLIT version 4 (Draxler and Hess, 1998) was employed to simulate the potential transport paths of the aeolian deposit in the three Red Clay sections during the late Miocene. The output from a Late Miocene global model simulation by Micheels et al. (2011) was used as the meteorological data to drive HYSPLIT. Three-dimensional 5-day backtrace trajectories of the near surface air mass (1000 m above ground level) of the three Red Clay localities were calculated every 12 hours for both winter (December, January, February) and spring (March, April, May). Finally, all the calculated trajectories were grouped into 4–5 mean trajectories to represent the dominant pathways of the air mass delivering dust to the studied Red Clay localities.

5 Summary of original papers

5.1 Paper I

The objective of paper was to investigate the spatiotemporal variations in the provenance of late Miocene-Pliocene Red Clay of the CLP. Three well-known Red Clay sequences in the CLP were examined: Baode in the northeast,

Lantian in the south and Dongwan in the west (Figs. 1 and 2 in Paper I). Firstly, an end-member modelling approach was applied to the grain-size distribution dataset of the three Red Clay sequences to characterise the subpopulations of the sediments and their relative contributions within the sections, and to understand the corresponding transport and depositional processes for the various components (Fig. 3 in Paper I). Subsequently, single-grain zircon U-Pb dating was used to explore the potential sources for the Red Clay (Figs. 4 and 5 in Paper I). Additionally, backtrace trajectory modelling was employed to investigate the transport pathways of the studied Red Clay localities and the prevailing wind patterns over the CLP in the late Miocene and Pliocene (Fig. 7 in Paper I).

It was revealed that the clay-dominated Red Clay of the southern (Lantian) and western (Dongwan) CLP was mainly derived from the NTP and Taklimakan Desert and was delivered by low level westerly winds. The more silt-dominated Red Clay in the northeastern CLP (Baode) is comprised of sediments transported from the NTP and a broad area of northern China (Central China Orogenic Belt) by northwesterly and northerly winds. The results are comparable to the dust supply pattern of the Quaternary loess, implying that a consistent spatial pattern variation in the provenance of the wind-blown sediments in the CLP started at least in the late Miocene. Temporally, Baode Red Clay in the NE CLP shows an increased source signature from the western deserts since 3.6 Ma. This might have resulted from the uplift of the Tibetan Plateau and Tianshan Mountains in the Pliocene, which intensified the westerly wind strength and/or aridity of western China. This could also be connected with the onset of enhanced drainage of the Yellow River promoted by increased denudation of the NTP since 3.6 Ma, which allowed more sediments to be delivered to the CLP by the Yellow River.

5.2 Paper II

The focus of this paper was on investigating the role of the Yellow River in supplying dust to the loess deposits and the mechanism behind the change in sedimentology of the loess-palaeosol sequence from the MLP along the lower reach of the Yellow River (Fig. 1 in Paper II). The sub-components of the Mangshan loess and its contributions within the bulk sediments were characterised by an end-member modelling approach applied to a grain-size distribution dataset (Figs. 2 and 3 in Paper II). A dust flux model was used to investigate the change in the dust accumulation rate along the sequence (Fig. 4 in Paper II). Fingerprinting of the source of Mangshan loess and its provenance variation was achieved by means of single-grain zircon U-Pb dating (Figs. 5 and 6 in Paper II).

The similarity of zircon U-Pb age components between the Mangshan loess and the Yellow River sediment suggests that loess deposits of the MLP have mainly been derived from the Yellow River floodplain north of the plateau. No obvious temporal variation has been found in the provenance signal of the Mangshan loess from loess units L9 to L1, indicating that the dust supply from the Yellow River floodplain to the MLP was initiated at least 900 ka (MIS22). This implies that the Yellow River cut though the Sanmen Gorge at least before 900 ka. Grain-size data and the dust flux model show that both the coarser-grained fraction and the dust accumulation rate have significantly increased in the upper Mangshan loess sequence above S2, suggesting increased sediment supply and a more proximal source for the MLP since 240 ka. The sudden change in sedimentology (grain size and accumulation rate) of the Mangshan loess around 240 ka is contemporaneous with tectonic movements in the Weihe Basin. This probably

suggests that due to tectonic uplift in the Weihe Basin around 240 ka, rapid fluvial incision in the basin caused tremendous amounts of fluvial sediments to be carried out of the Sanmen Gorge to the lower reach of the Yellow River, leading to the formation of a larger fluvial fan north of the MLP and resulting in increased dust being transported to MLP via aeolian processes. Moreover, the southern migration of the Yellow River evidenced by a northern high scarp of the MLP probably provided a more proximal source area for the MLP during the middle and late Pleistocene.

5.3 Paper III

This paper aimed to fingerprint the transport process of the silt (2–63 μm) particles in the late Neogene and Quaternary aeolian sediments (Red Clay and loess) of the CLP by applying dynamic image analysis (DIA; Sympatec Qicpic) in the characterisation of the grain-size and grain-shape distribution. Samples were collected from four Quaternary loess sections, namely Huanxian, Xifeng, Xunyi and Duanjiapo, along a north-to-south transect in the CLP and from three Red Clay sequences distributed across the CLP: Baode in the northeast, Lantian in the south and Dongwan in the west (Fig. 1 in Paper III) .

The grain-size distribution of the samples was measured both by DIA and laser diffraction (LD) particle-size analysis (Fig. 4 in Paper III). Similarly to the grain-size dataset produced LD, DIA characterisation of the grain-size distribution of Quaternary loess not only differentiated the glacial loess units from interglacial palaeosol units, but also revealed clear spatial variation, with the grain size decreasing from the northern to the central and southern parts of the CLP during the last two glacial and interglacial cycles. A similar spatial pattern was also revealed by DIA for the fine-grained Miocene-Pliocene Red Clay. Moreover, DIA was able to characterise the fluvial contribution to the Red Clay, as indicated by different grain-size and grain-shape distribution curves. The grain-shape analysis of DIA revealed a systematic pattern for both the loess-palaeosol sequences and Red Clay sediments, whereby the aspect ratio decreased as a function of increasing grain size. This probably suggests that systematic shape sorting occurred during the aeolian transportation of the silt particles. We found that certain grain-size ranges corresponded to specific aspect ratios that seemed to be aerodynamically distinguishable from each other and that could be further linked to the wind velocity/strength in transporting the particles.

5.4 Paper IV

The aim of this paper was to introduce a new approach for characterising the provenance of detrital quartz from the loess and Red Clay deposits using laser-ablation inductively coupled plasma-mass spectrometry (ICP-MS). Trace elements in quartz were analysed from Quaternary loess samples of the Mangshan Plateau in central China, late Miocene-Pliocene Red Clay samples of the Baode section in the northeast of the CLP and sand dune samples from the major deserts in northern and western China (Figs. 1 and 2 in Paper IV). Three trace elements (Li, Ti and Sc) in quartz are presented (Fig. 3 in Paper IV) and the data indicate that the Qaidam Basin has a similar trace element distribution in quartz to that in Quaternary loess, implying a significant contribution of debris from the Qaidam Basin to the loess deposits of northern China. The data also suggest a possible dust supply from the Taklimakan Desert to the Baode Red Clay, as demonstrated by the similarity of the Ti and Sc contents in the quartz grains (Fig. 4 in Paper IV). The provenance signature indicated by the Ti and Sc contents

of quartz in general are consistent with the previous interpretation based on zircon U-Pb ages. It is suggested that the Sc content in quartz might be a potential source indicator for aeolian loess and Red Clay.

6 Discussion

6.1 Variations in the provenance of the CLP dust

The provenance analysis for the three Red Clay sequences across the CLP indicated that debris sourced from the NTP accounts for the majority of the dust supply for the late Miocene-Pliocene Red Clay (Paper I). A spatial pattern probably existed for the provenance of the Red Clay deposits, because sites of the western and southern CLP show a strong source affinity with the west (NTP and Taklimakan Desert), while the northeastern CLP received more sediments from the broad area in the Central Asia Orogenic Belt (CAOB), including the distant Gobi Altay Mountains and proximal North China Craton. Previous studies have revealed that Quaternary loess deposits are also derived from multiple source areas, with sediments eroded from the regions west of the CLP, i.e. the northern and/or northeastern Tibetan Plateau appearing to be dominant (Bird et al., 2015; Licht et al., 2016a; Pullen et al., 2011; Stevens et al., 2010; Zhang et al., 2016). The spatial variation in the provenance of the Red Clay across the CLP is thus comparable with the Quaternary loess, as indicated by Bird et al. (2015), suggesting that such a dust supply pattern, combining western and northern sources, has been consistent at least since the late Miocene (~7 Ma). In addition, unlike the Quaternary loess, the work presented in this PhD thesis addressed the likely source contribution from the distant Taklimakan Desert to the Red Clay sequences (Papers I and IV). The provenance study of the central CLP Red Clay also indicated that the early Pliocene Red Clay (5.5–4 Ma) was primarily derived from the distal Taklimakan Desert (Nie et al., 2014). Considering the finer nature of Red Clay sediments, which are mainly composed of clay-silt particles, a more distal source for the Red Clay is possible. However, it should be pointed out that both the Taklimakan Desert and the NTP lie west of the CLP, along the dust-transporting westerly wind track, and that their provenance characteristics both share (overlapping) dominant zircon age populations (200–300 and 400–500 Ma). Dust entrained from the Taklimakan desert could therefore be mixed with sediments from the Qaidam Basin and the Qilian Mountains of the NTP, and cannot be effectively distinguished based only on the source signal of zircon U-Pb ages. The Red Clay site from Baode in the northeastern CLP suggested possible temporal variation for the provenance of Red Clay deposits by showing increased dust input from the western deserts since 3.6 Ma (Paper I). Nie et al. (2014) also demonstrated that the upper part of the late Pliocene Chaona Red Clay in the central CLP is dominated by the western sources of the NTP. Together, this implies a prominent western source for the CLP dust since the late Pliocene (3.6 Ma).

It is still under debate whether the provenance of the CLP loess varied systematically on a spatial and/or a temporal scale (Bird et al., 2015; Che and Li, 2013; Nie et al., 2015; Xiao et al., 2012). Using zircon U-Pb age spectra as a source signature, Xiao et al. (2012) found that the zircon age signals of the loess units are different from those of palaeosol units, suggesting that the provenance of CLP loess changed over glacial–interglacial cycles. They ascribed such variation to the different atmospheric circulation patterns during glacial and interglacial periods,

as the mean annul position of the polar jet stream shifted about 10° towards the equatorial during glacial periods (Kapp et al., 2011; Pullen et al., 2011). Their results also indicated spatial differences in the provenance of the aeolian deposits of the CLP, particularly for the interglacial palaeosol unit: the palaeosol unit S1 showed an eastward increase in the dust source from northern China and southern Mongolia. However, Che and Li (2013) argued that there are no temporal or spatial heterogeneities in the zircon age distribution in the CLP loess deposits, and they questioned the results of Xiao et al. (2012), which might be uncertain due to the small sample size. They proposed binary sources for the CLP mixing sediments from the NTP and the GAM (Che and Li 2013). The Alxa arid lands, which receive material from both the NTP and the GAM, comprise the main source area for the CLP loess (Fig. 1 and Fig. 7). The results of Bird et al. (2015) demonstrated spatial heterogeneity of the loess deposits across the CLP: loess deposits in the western CLP show a strong genetic link to the Yellow River and the NTP, while the eastern CLP loess receives greater contributions from the North China Craton source. They also found that the provenance of the loess deposits varied over time, but the shifts were not consistent with the changes in the glacial and interglacial cycles. A recent study by Licht et al. (2016a) revealed that the zircon age distribution of palaeosol layers is similar to that of the loess layers. However, they concluded that this is because interglacial palaeosol deposits could be reworked old glacial loess that has homogenised the source signals. The provenance analysis of the loess-palaeosol sequence in the MLP presented in Paper II showed that the Mangshan loess deposits have been consistently supplied from the local (lower reach) Yellow River floodplain from L9 to L1 (last 900 kyrs), with no significant provenance signal changes. However, this work only focused on the zircon U-Pb dating of the loess units. Further study of the palaeosol units may be needed to investigate whether any glacial–interglacial variations exist in the provenance of Mangshan loess-palaeosol sequence.

6.2 Yellow River and CLP dust

Penck (1931) already pointed out the Yellow River as the primary transporter of the CLP loess decades ago. However, it is not until recent years that provenance studies based on single-grain zircon U-Pb dating have provided diagnostic evidence for a possible genetic link between the upper reach sediments of the Yellow River and the CLP loess deposits (Nie et al., 2015; Stevens et al., 2013). Licht et al. (2016a) and Zhang et al. (2016) further demonstrated that reworked Yellow River sediments contribute more than 60% to the aeolian dust supply of the CLP. Our provenance analysis of Mangshan loess deposits in the lower reach of the Yellow River provided the same information that the Yellow River floodplain north of the MLP has served as a major dust source for the Mangshan loess deposits (Paper II).

Pye (1995) has pointed out that more than one phase of fluvial and subsequent aeolian transport could be involved in the production of loess sediments. In the case of the Mangshan loess deposited during (at least) the last two glacial and interglacial intervals, it can be inferred that at least two phases of fluvial-aeolian processes took place in transporting the sediments from the source area (i.e. the NTP) to the MLP (Fig. 7): firstly, detrital sediments eroded from the NTP were carried by the upper reach of the Yellow River to the Yinchuan-Hetao Graben, and from there were delivered by the winter monsoon winds to the Mu Us Desert and then

to the CLP (Bird et al., 2015; Nie et al., 2015; Stevens et al., 2013); secondly, loess deposits in the central CLP were cannibalised by fluvial erosion in the drainage system in the Weihe Basin and carried to the lower reach of the Yellow River through the Sanmen Gorge. These fluvial sediments were again reworked by aeolian processes and transported by northerly near-surface winds to the MLP. It can be seen that the interaction of the Yellow River and CLP dust is a dynamic process in which the upper reach of the Yellow River can be considered as a temporary source of the CLP dust that brought sediments from the high mountains to the area upwind of the CLP, while in the middle reach, the river acted as a net remover for the CLP sediments, carrying large amounts of silts from the Weihe Basin through the Sanmen Gorge to the broad alluvial fan system of the NCP in the lower reach of the Yellow River. Eventually, the lower reach of the Yellow River (floodplain) acted (again) as source for the dust deposits of its downwind area (i.e. MLP) (Fig. 7).

This PhD study has shed light on the evolution of the Yellow River. Topics such as when the channel connecting the middle and lower reaches of the Yellow River developed, and questions such as "When did the Yellow River cut through Sanmen Gorge?" or "When did the Sanmen palaeolake drain?" have been actively debated (Hu et al., 2012, 2017; Kong et al., 2014; Wang, 2002; Zhang et al., 2004; Zheng et al., 2007). Thermoluminescence dating of the fluvial terrace sands in the Sanmen Gorge has suggested that the Sanmen palaeolake drained at 0.15 Ma and resulted in a dramatic increase in the sediment accumulation rate in the Mangshan loess deposits (Jiang et al., 2007; Wang, 2002; Zhang et al., 2004). However, the newly established age model for the Mangshan loess-palaeosol sequence demonstrated that Mangshan palaeosol unit S2 is equivalent to the marine isotope stage 7 (243–191 ka) and implied that the Sanmen palaeolake drained before palaeosol unit S2 was formed (Qiu and Zhou, 2015; Zheng et al., 2007). A strong piece of evidence based on the dating of the fluvial terrace along the Sanmen Gorge indicated that the incision of the Yellow River through the Sanmen Gorge took place at least before 1.2 Ma (Hu et al., 2012, 2017). Based on the zircon U-Pb age

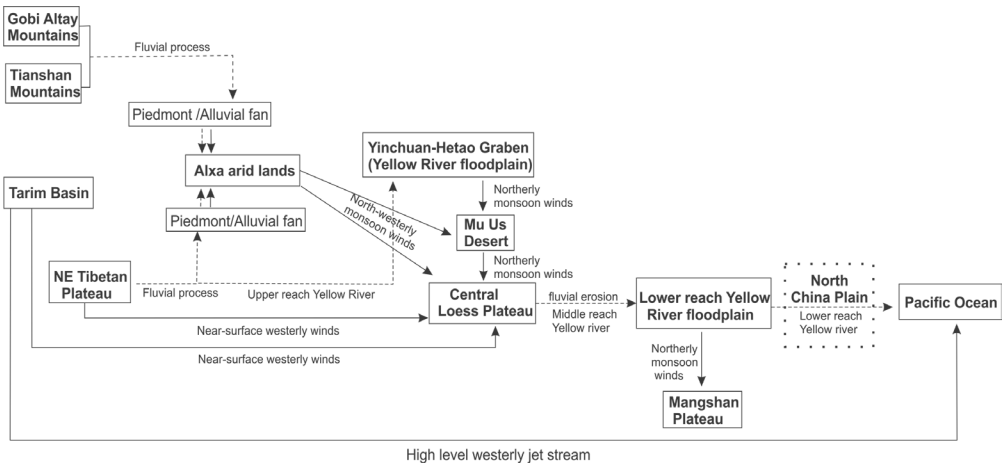

Figure 7. Sediment provenance and transport pathways from the Asia interior to the Pacific Ocean. Dashed arrows indicate the fluvial processes and solid arrows indicate the aeolian processes.

chronology and nuclide burial dating of the fluvial sediments in the Sanmen Basin, Kong et al. (2014) concluded that the transition from a lacustrine to a fluvial environment in the Sanmen Basin occurred at 1.3–1.5 Ma. Rits et al. (2017) concluded that the Sanmen palaeolake in the eastern part of the Weihe Basin did not exist during the last 1 Myr. This PhD study provided provenance evidence that the Yellow River floodplain north of the MLP has been a constant dust supplier for the Mangshan loess deposits at least since 900 ka, indicating that the Yellow River cut through the Sanmen Gorge before 900 ka. These results are in accordance with Hu et al. (2012, 2017), Kong et al. (2014) and Rits et al. (2017), supporting the early Pleistocene ages of the Yellow River incision through the Sanmen Gorge.

6.3 Transport and deposition of loess and Red Clay

It has been proposed that two types of processes are mainly involved in the transport of aeolian loess sediments: the coarse silt and fine sand fraction are generally transported by surface winds in short suspension and saltation and deposited in proximal areas; by contrast, the fine silt and clay fraction, once lifted into the atmosphere, can be transported by high level flow from distant source areas (Pye, 1995; Pye and Zhou, 1989; Tsoar and Pye, 1987). Prins and Vriend (2007), Prins et al. (2007) and Vriend et al. (2011) conducted end-member modelling of the grain-size distribution of loess-palaeosol sequences in the central CLP and revealed that the loess sediments are comprised of three unimodal and fine-skewed end members: clayey EM1, silty EM2 and sandy EM3, with mode sizes of 63 μm, 37 μm and 22 μm, respectively. It has been shown that the sandy EM1 decreased from the northern CLP to the distal southern region, while the clayey EM3 increased from the north to the south. Prins et al. (2007) further interpreted that the coarse EM1 and EM2 are supplied by northerly and/or northwesterly winter monsoon winds during major spring and early summer dust storms via saltation and short-term suspension processes over the proximal region of the CLP. The clayey fraction EM3 is considered as a background dust system that has constantly been supplied via long-term suspension by westerly winds during interglacial stages, and it could also have been accompanied by major dust outbreaks through transport by the winter monsoon during glacial stages. The unmixing model of the grain-size distribution of Mangshan loess provided the same results: Mangshan loess sediments contain three end members that are comparable to the distribution of the central CLP loess (Fig. 3 in Paper II). This implies a similar aeolian transport pattern for the Mangshan loess as the central CLP loess. However, the modal size of the clayey EM1 of the Mangshan loess is 26 μm, which is coarser than the modal grain size of the CLP loess (EM3 modal size 22 μm). This suggests a more proximal source area for the Mangshan loess compared to the CLP loess, and is in agreement with the provenance evidence that the Mangshan loess deposits have mainly been supplied by the Yellow River floodplain from its north.

In this work, the end-member modelling approach was applied to investigate the subcomponents of the late Neogene Red Clay deposits (Paper I). A similar spatial distribution pattern to the loess is present in Red Clay deposits: Red Clay in the northeastern CLP is more silt dominated, while the southern CLP Red Clay contains more of the clayey fraction. However, the end-member grain-size distribution of Red Clay is more complex. It is characterised by a clear bimodal grain-size

distribution that was found to vary between sites (Fig. 3 in Paper I). The results confirmed that the main part of the Red Clay was transported by aeolian processes, but it also pointed out a fluvial contribution to the Red Clay deposits, as indicated by high proportions of the sandy EM1 in the bottom part of the Baode Fm and Lantian Fm. The bimodal clayey end members in the Red Clay deposits are noteworthy. Prins et al. (2007) indicated that the clayey EM3 in the loess may have been formed during the pedogenic process after deposition, which increased the proportion of the clayey fraction in the southern CLP. Compared to the loess deposits, Red Clay is a much finer sediment, dominated by fine silt and clay fractions. The distinct reddish colour and occurrence of Fe-Mn nodules indicate the sediments have experienced strong weathering processes in a relatively warm and humid environment. Earlier, Sun et al. (2006) already suggested that the grain-size distribution of Red Clay may have been altered by post-depositional pedogenic processes. Hence, the bimodal distribution of the clayey end member in Red Clay could result from weathering, resulting in a mix of aeolian mineral grains and clay minerals produced *in situ*. Furthermore, field observations revealed that the Red Clay of the Lantian Fm and Jingle Fm (Baode) has suffered a more intensive pedogenic process than the deposits of Dongwan and the Baode Fm (Guo et al., 2002; Kaakinen, 2005; Li et al., 2014; Zhang et al., 2013; Zhu et al., 2008). The results of this work indicate that the proportion of the bimodal clayey end member in the Lantian Fm and Jingle Fm is much higher than in the Dongwan Red Clay (clayey EM3 of the Baode Fm is polymodal, and thus not compared). Therefore, this probably confirms, in agreement with the field observations, that the bimodal clayey end member in the Red Clay is a proxy for the degree of weathering.

Dynamic image analysis of grain size and grain shape was used to further investigate the detailed transport pattern of loess and Red Clay deposits. Grain shape, another principal property for sediments next to grain size, has been less investigated in the aeolian sedimentary deposits. This study revealed a systematic distribution pattern of grain size and grain shape for the CLP dust: the aspect ratio increases as a function of decreasing particle size, particularly for the silt-sized particles (20–60 μm), in loess, palaeosol and Red Clay sediments (Paper III). This suggests that small particles are more symmetric or spherical in shape than large particles within this silt-size fraction. The implication is that systematic wind sorting has occurred during the transportation of silt particles, and their distribution pattern probably provides information on the suspension process and the fall velocity of the particles. From this work, it could follow that these typical particle shape–size relationships can be used in defining aerodynamic end members for the reconstruction of wind strength and velocity.

6.4 Climate and tectonic controls on the dust supply of the CLP loess and Red Clay

For the continuous accumulation of aeolian sediments, there are three prerequisites according to Pye (1995): "1) arid source area(s) with bare and unstable geomorphic surface composed of poorly sorted sediments with a high silt/clay ratio, 2) a high frequency of strong turbulent winds and 3) a suitable accumulation site."

Under such a rationale, the deposition of loess-palaeosol and the Red Clay sequence since the Oligocene in the CLP has been correlated with the long-term aridity of the Asia interior and the onset of and changes in the Asian monsoon system (An et al., 2001; Guo et al., 2002). Two

prominent events occurred during the Cenozoic in Eurasia: the retreat of the Paratethys Sea and the uplift of the Tibetan Plateau, both as a result of the India–Asia continental collision. These two events significantly changed the land–sea distribution, triggering intensive aridification and cooling of continental Asia, and the onset of the Asian monsoon, although the detailed mechanism remains controversial (Dupont-Nivet et al., 2008; Harris, 2006; Liu et al., 2003; Raymo and Ruddiman, 1992; Zhang et al., 2007). It has been considered that the uplift of the Tibetan Plateau and Tianshan Mountains prompted erosion and weathering of the bedrock, which provided considerable volumes of sediments to the mountain foothills in the form of alluvial fans, serving as the dust sources for the CLP (loess) deposits (Fig. 7). In addition, the growth of the Tibetan Plateau has separated the westerly jet into a northern and southern branch. The northern branch, which flows along the edge of the NTP and through Asia's dry interior, acts as a major medium for long-term dust transport from the Asian interior to the Pacific Ocean (Fig. 7). The Tibetan Plateau uplift has also blocked moisture from the Indian Ocean, further enhancing the aridity in the interior of Asia. In addition, the stabilised Ordos Block since the late Miocene might have provided a suitable accumulation platform for continuous dust deposition in the central CLP (Wang et al., 2017), as most of the completed loess-palaeosol-Red Clay sequence with basal ages after 8 Myr has been found in the Ordos Block (Ding et al., 1998; Sun et al., 1997).

According to the results of this work, the dust supply from the NTP and Taklimakan Desert started from 7 Myr ago, indicating aridity in western China at least since the late Miocene (Paper I). Other evidence based on the ostracod fauna, stable isotopes and palaeo-weathering indices also indicates that the Qaidam Basin has experienced increasing aridity since 13.3 Ma due to the uplift of the Tibetan Plateau (Song et al., 2017). Zheng et al. (2015) proposed a late Oligocene-early Miocene formation age for the Taklimakan Desert. This implies the possibility of dust supply from the far west since the late Oligocene. A recent study further demonstrated that desert expansion and aeolian dust generation in the Asia interior may have taken place much earlier by confirming the presence of Eocene aeolian dust in the northeastern boundary of the Tibetan Plateau (Licht et al., 2016b).

The present work also revealed noticeable variation in the provenance of Red Clay since 3.6 Ma. The dust supply from the arid lands of western China has probably increased since 3.6 Ma, which could have been caused by strengthened westerly winds and/or aridity in western China during the Pliocene. Supportive evidence from climate modelling simulations showed enhanced westerly winds as a consequence of the uplift of the NTP in the Pliocene (Zhang et al., 2015). Proxy records based on pollen and geochemical data have also documented intensified aridity in the Qaidam Basin and Taklimakan Desert (Liu et al., 2014; Sun et al., 2015; Wu et al., 2011). Nie et al. (2015) proposed that the sediments derived from the NTP have largely been stored in the CLP and western Mu Us Desert since 3.6 Ma due the increased erosion of the NTP. Therefore, the increased denudation of the NTP and consequently enhanced Yellow River drainage since 3.6 Ma could also have contributed to the increased sediment supply to the CLP since this time.

On a more regional scale, as witnessed in the Mangshan Plateau loess sections, tectonic activity is also probably a dominant factor in controlling loess deposition. The trend of a dramatic increase in the sedimentation rate and coarser sediment flux (silt and fine sand

component) occurred above palaeosol unit S2 (240 ka) (Paper II). The timing coincides with increased fluvial incision caused by tectonic motions in the Weihe Basin upstream of the MLP (Fig. 1) (Rits et al., 2017). A study on the river terraces in the middle reach of the Yellow River in the eastern part of the Weihe Basin also revealed a significantly increased incision rate of the Yellow River due to the local tectonic uplift. Therefore, it is likely that the tectonic uplift/movements triggered the increased fluvial incision in the Weihe Basin and middle reach of the Yellow River at around 240 ka. This resulted in an increased sediment flux being transported to the lower reach of the Yellow River and, as a consequence, enlarged the alluvial fan of the Yellow River in its lower reach north of the MLP. Since this fan serves as the major dust supply for the MLP, the sedimentation flux and coarser grain component dramatically increased. In addition, local fault movements that resulted in the southern migration of the Yellow River towards the MLP could also have contributed to the sedimentology change of the Mangshan sequences by providing a more proximal source area.

6.5 Application of novel techniques in studying the provenance and transport of the CLP aeolian dust

One of the main efforts of this work was the application of novel analytical approaches in studying the provenance and transport of past aeolian sediments. It was the first time that DIA had been used to characterise the grain size and shape of the silt particles (2–63 μm) in the loess and Red Clay deposits of northern China (Paper III). The grain size results yielded from the DIA showed that during the last two glacial–interglacial cycles, the coarse silt (>32 μm and <63 μm) and fine sand fraction (>125 μm) in the loess-palaeosol sequence decreased from the northern CLP to the southern CLP sites. The gradient of the southward decreasing trend is more dramatic in glacial periods than interglacial periods (Fig. 6 in Paper III). These results are comparable to the grain-size distribution pattern yielded from the LD analysis (Fig. 4 and Fig. 5 in Paper III). Therefore, this study demonstrated that DIA is able to precisely measure the grain size of aeolian silt particles. In addition to the grain size, DIA can also provide information on particle shape, as discussed in section 6.3. However, the fraction <16 μm in the loess and Red Clay tends to be underestimated by DIA due to the resolution of the camera (pixel size 2 × 2 μm) used in this study. Therefore, the smallest size for precise analysis of particles is 16 μm based on the current device setting. This is consistent with results for Belgian loess reported by Tysmans et al. (2006), who similarly found the accuracy of measurement to be better for larger particles (>20 μm). In the future, it is to be expected that by increasing the resolution of the camera, finer particles will be more precisely measured by DIA.

In this study, quartz geochemistry was also used as a provenance signature to trace the dust sources of aeolian loess and Red Clay deposits (Paper IV). The trace element content of Li, Ti and Sc in single quartz grains from loess, Red Clay and deserts sands of the potential source areas, i.e. the Mu Us Desert, Tengger Desert, Qaidam Basin and Taklimakan Desert, were analysed by ICP-MS laser ablation. It was found that the trace element signature of Mangshan loess showed close affinity with that of the Qaidam Basin. The possible contribution of the Taklimakan Desert to the Baode Red Clay is also indicated by the similar trace element contents of quartz. These results are consistent with the provenance study based on zircon U-Pb ages, thus indicating that trace elements in quartz grains could be used as a potential

tool for the provenance study of past aeolian sediments. However, it should be mentioned that as a preliminary study, the results of this work were based on a relatively small number of analysed samples. The quantity of quartz grains used for statistical comparison after data reduction varied from 37 to 118 (lower than the average statistics as used in the zircon U-Pb dating). As a consequence, the presented data might only partly comprise the source information. Systematic provenance analysis based on large number of samples from both the potential source areas and loess and Red Clay sites is required in order to better constrain the source supplies of the aeolian deposits of the CLP.

6.6 Limitations and future outlook

The study based on zircon U-Pb chronology has advanced knowledge of the dust sources of the CLP aeolian deposits. An extensive provenance dataset has already been established for the Quaternary loess sediments (Bird et al., 2015; Che and Li, 2013; Licht et al., 2016a; Pullen et al., 2011; Stevens et al., 2010; Xiao et al., 2012), which allows for detailed quantification of contributions from multiple source areas, as well the shift in the dust supply through time and space. For the Miocene-Pliocene Red Clay sequences, of which the lithology is more variable between sites, the provenance analysis is still limited to a few sections (Gong et al., 2016 and Paper I; Nie et al., 2014). Further zircon U-Pb chronology studies based on a high temporal resolution of multiple Red Clay sites is needed in order to fully investigate the spatial and temporal variation in the sources of the Red Clay deposits. It should also be noted that the particle size range of the zircon grains used for provenance dating of the CLP dust and the material from the potential source regions was not consistent: zircon grains from the desert sample usually yielded a larger grain size range of 50–100 μm and were measured with a laser spot size of 30–55 μm (Stevens et al., 2010; Zhang et al., 2016), while zircons from loess and Red Clay deposits were most abundant in the silt fraction of 20–60 μm and were analysed with a laser spot size of 12–25 μm (Che and Li, 2013; Licht et al., 2016a; Pullen et al., 2011). Grain size, next to density, is one of the main factors affecting the transportation distance of the dust deposits. It would be worthwhile to investigate the provenance signature of material from the source regions having the same size range as the aeolian deposits in the CLP, if possible. In addition, systematic and detailed provenance analysis is also required for the potential source areas. While the source regions such as the NTP and the proximal deserts, i.e. the Mu Us Desert and Tengger Desert, have received considerable attention, there is relatively less provenance data from distal regions such as the Mongolian Gobi Desert and the Tarim Basin. There is also uncertainty regarding the provenance interpretation based on zircon U-Pb age spectra due to the overlap of dominant zircon age populations in the potential sources. For example, both the Taklimakan Desert and the NTP contain two prominent zircon age components at 200–300 Ma and 400–500 Ma (Pullen et al., 2011; Rittner et al., 2016). Paper I might have provided a good example in resolving the issue. A combination of provenance data and dust trajectory simulation will help to determine the detailed dust transport pathway and quantify the mixed contributions from the multiple sources. Moreover, Paper IV demonstrated the potential of using trace elements in detrital quartz to fingerprint the source of the CLP dust. The development/improvement of such a new provenance signature is needed, and the multiple source indictors could be combined to obtain a complete picture of the dust transport

pathways of the aeolian deposits and to reduce the bias that might be induced from observations and interpretation based on a single provenance indicator.

End-member modelling of the grain size dataset of loess and palaeosol sequences revealed that silt and fine sand fractions are supplied from proximal regions, while the clay fraction might be transported from more distal area(s). The provenance study of this work was mainly focused on the silt fraction of the loess and Red Clay deposits, with the analysed zircon grains being in the size range of 20–60 μm. The origin of the finer clayey fraction in the loess and Red Clay deposits is beyond the scope of this work. In the future, comprehensive provenance analyses covering both the coarser and finer component of the loess and Red Clay sediments will be valuable in fully understanding the dust supply pattern of the late Neogene and Quaternary dust deposits in northern China. In addition, the observations and simulations of modern dust emission and transport will be useful in investigating the past dust transport processes. Empirical data such as the dust loading capacity of the airflow and the wind velocity in entraining dust from the ground to the air are highly demanded in explaining and reconstructing the past wind strength and dust transport pattern.

7 Concluding remarks

In this work, single-grain zircon U-Pb dating, dynamic image analysis of grain size and grain shape, end-member modelling of the grain-size distribution dataset and the trace element content in quartz were used to fingerprint the dust source and transport process of the late Neogene and Quaternary aeolian deposits in northern China. The main findings and implications of the study can be summarised as follows:

(1) As revealed by zircon U-Pb age components, the late Miocene-Pliocene Red Clay is ultimately supplied from the NTP and the broad area of the CAOB (including the North China Craton and the Gobi Altay Mountains), with the former being more dominant; Red Clay sites in the southern and western CLP receive more dust from the western deserts, while NE CLP Red Clay shows a strong source affinity to the northern China Craton and Gobi Altay Mountains. Spatially, the dust supply pattern for the late Miocene–Pliocene Red Clay is similar to the Quaternary loess, indicating a Quaternary-like atmospheric pattern for the late Miocene in northern China. The uplift of the Tibetan Plateau and Tianshan Mountains in the Pliocene intensified the aridity of the Asia Interior. The growth of the Tibetan Plateau also resulted in the increased denudation of the Northern Tibetan Plateau and the onset of increased drainage of the Yellow River, and finally increased the sediment supply from the west to the CLP dust deposits.

(2) The zircon U-Pb age also revealed a genetic link between the Yellow River sediments and the Pleistocene loess in the MLP of northern central China, and indicated that the lower reach the Yellow River floodplain north of the MLP has served as a dominant source area for the loess deposits of the MLP at least since 900 ka. This further implied that the integration of the middle and lower reaches of the Yellow River took place earlier than 900 ka.

(3) On a regional scale, tectonic activity is the main driver for the change in dust deposition in the MLP. The dramatically increased coarse grain-size fractions and sedimentation rate in the loess-palaeosol sequence of the MLP since 240 ka were caused by tectonic movements of the Weihe Basin and vertical motions of the local faults. The tectonic uplift resulted in rapid erosion in the Weihe Basin and led to a large

volume of silts being delivered downstream of the Sanmen Gorge at about 240 ka, and resulted in the formation of a larger fluvial fan in the lower reach of the Yellow River. A more proximal source area for the Mangshan dust was established due to the southern migration of the Yellow River, which resulted from the vertical motion of the faults in the subsurface.

(4) Dynamic image analysis of grain size and shape demonstrated that the silt particles in the loess, palaeosol and Red Clay sediments exhibited a uniform grain size and shape distribution. The aspect ratio of the particles decreased as a function of increasing grain size, indicating that systematic shape sorting occurred during the aeolian suspension transport of silt particles and further confirming the preliminary aeolian origin of the Red Clay deposits.

(5) End-member modelling of the grain-size distribution of loess and Red Clay sediments indicated that the aeolian deposits in the CLP are probably a mixture of several different dust subpopulations that have been subjected to different transport processes. The finest clayey end member in the Red Clay deposits might have been altered by post-depositional processes.

(6) The trace element content in detrital quartz showed a similar provenance signature to the single-grain zircon U-Pb age data, and could potentially be used as an indicator for the provenance signature of the aeolian dust.

References

AFSOM, 1988. Active Fault System Around Ordos Massif. Seismological Press, Beijing.

Alonso-Zarza, A.M., Zhao, Z., Song, C.H., Li, J.J., Zhang, J., Martín-Pérez, A., Martín-García, R., Wang, X.X., Zhang, Y., Zhang, M.H., 2009. Mudflat/distal fan and shallow lake sedimentation (upper Vallesian–Turolian) in the Tianshui Basin, Central China: Evidence against the late Miocene eolian loess. Sedimentary Geology 222, 42-51.

An, Z.S., Kutzbach, J.E., Prell, W.L., Porter, S.C., 2001. Evolution of Asian monsoons and phased uplift of the Himalaya-Tibetan plateau since Late Miocene times. Nature 411, 62-66.

An, Z.S., Sun, Y.B., Zhou, W.J., Liu, W.G., Qiang, X.K., Wang, X.L., Xian, F., Cheng, P., Burr, G.S., 2014. Chinese Loess and the East Asian Monsoon, In: An, Z.S. (Ed.), Late Cenozoic Climate Change in Asia: Loess, Monsoon and Monsoon-arid Environment Evolution. Springer Netherlands, pp. 23-143.

Balkanski, Y., Schulz, M., Claquin, T., Guibert, S., 2007. Reevaluation of Mineral aerosol radiative forcings suggests a better agreement with satellite and AERONET data. Atmospheric Chemistry and Physics 7, 81-95.

Belousova, E.A., 2005. Zircon Crystal Morphology, Trace Element Signatures and Hf Isotope Composition as a Tool for Petrogenetic Modelling: Examples From Eastern Australian Granitoids. Journal of Petrology 47, 329-353.

Bird, A., Stevens, T., Rittner, M., Vermeesch, P., Carter, A., Andò, S., Garzanti, E., Lu, H., Nie, J., Zeng, L., Zhang, H., Xu, Z., 2015. Quaternary dust source variation across the Chinese Loess Plateau. Palaeogeography, Palaeoclimatology, Palaeoecology 435, 254-264.

Blott, S.J., Pye, K., 2001. GRADISTAT: a grain size distribution and statistics package for the analysis of unconsolidated sediments. Earth Surface Processes and Landforms 26, 1237-1248.

Che, X., Li, G., 2013. Binary sources of loess on the Chinese Loess Plateau revealed by U–Pb ages of zircon. Quaternary Research 80, 545-551.

Chen, J., Li, G., Yang, J., Rao, W., Lu, H., Balsam, W., Sun, Y., Ji, J., 2007. Nd and Sr isotopic characteristics of Chinese deserts: Implications for the provenances of Asian dust. Geochimica et Cosmochimica Acta 71, 3904-3914.

Chen, Z., Li, G., 2013. Evolving sources of eolian detritus on the Chinese Loess Plateau since early Miocene: Tectonic and climatic controls. Earth and Planetary Science Letters 371-372, 220-225.

Cheng, H., Edwards, R.L., Broecker, W.S., Denton, G.H., Kong, X., Wang, Y., Zhang, R., Wang, X., 2009. Ice age terminations. Science 326, 248-252.

Cheng, H., Edwards, R.L., Sinha, A., Spotl, C., Yi, L., Chen, S., Kelly, M., Kathayat, G., Wang, X., Li, X., Kong, X., Wang, Y., Ning, Y., Zhang, H., 2016. The Asian monsoon over the past 640,000 years and ice age terminations. Nature 534, 640-646.

Craddock, W.H., Kirby, E., Harkins, N.W., Zhang, H., Shi, X., Liu, J., 2010. Rapid fluvial incision along the Yellow River during headward basin integration. Nature Geoscience 3, 209-213.

Crusius, J., Schroth, A.W., Gassó, S., Moy, C.M., Levy, R.C., Gatica, M., 2011. Glacial flour dust storms in the Gulf of Alaska: Hydrologic and meteorological controls and their importance as a source of bioavailable iron. Geophysical Research Letters 38, L06602.

Dentener, F.J., Carmichael, G.R., Zhang, Y., Lelieveld, J., Crutzen, P.J., 1996. Role of mineral aerosol as a reactive surface in the global troposphere. Journal of Geophysical Research: Atmospheres 101, 22869-22889.

Deplazes, G., Lückge, A., Stuut, J.-B.W., Pätzold, J., Kuhlmann, H., Husson, D., Fant, M., Haug, G.H., 2014. Weakening and strengthening of the Indian monsoon during Heinrich events and Dansgaard-Oeschger oscillations. Paleoceanography 29, 99-114.

Ding, R., 2005. Decadal change of the spring dust storm in northwest China and the associated atmospheric circulation. Geophysical Research Letters 32, L02808.

Ding, Z.L., Derbyshire, E., Yang, S.L., Yu, Z.W., Xiong, S.F., Liu, T.S., 2002. Stacked 2.6-Ma grain size record from the Chinese loess based on five sections and correlation with the deep-sea $\delta^{18}O$ record. Paleoceanography 17, doi: 10.1029/2001PA000725.

Ding, Z.L., Sun, J.M., Liu, T.S., Zhu, R.X., Yang, S.L., Guo, B., 1998. Wind-blown origin of the Pliocene red clay formation in the central Loess Plateau, China. Earth and Planetary Science Letters 161, 135-143.

Ding, Z.L., Sun, J.M., Yang, S.L., Liu, T.S., 2001a. Geochemistry of the Pliocene red clay formation in the Chinese Loess Plateau and implications for its origin, source provenance and paleoclimate change. Geochimica Et Cosmochimica Acta 65, 901-913.

Ding, Z.L., Yang, S.L., Hou, S.S., Wang, X., Chen, Z., Liu, T.S., 2001b. Magnetostratigraphy and sedimentology of the Jingchuan red clay section and correlation of the Tertiary eolian red clay sediments of the Chinese Loess Plateau. Journal of Geophysical Research-Solid Earth 106, 6399-6407.

Draxler, R.R., Hess, G.D., 1998. An overview of the HYSPLIT_4 modeling system of trajectories, dispersion, and deposition. Australian Meteorological Magazine 47, 295-308.

Dupont-Nivet, G., Hoorn, C., Konert, M., 2008. Tibetan uplift prior to the Eocene-Oligocene climate transition: Evidence from pollen analysis of the Xining Basin. Geology 36, 987-990.

Flynn, L., Wu, W.-Y., 2017. Late Cenozoic Yushe Basin, Shanxi Province, China: Geology and Fossil Mammals. Volume II: Small Mammal Fossils of Yushe Basin. Springer.

Flynn, L.J., Deng , T., Wang, Y., Xie, G.-P., Hou, S.-K., Pang, L.-B., Wang, T.-M., Mu, Y.-Q., 2011. Observatons on the Hipparion Red Clays of the Loess Plateau. Vertebrata PalAsiatica 49, 275-284.

Gong, H., Nie, J., Wang, Z., Peng, W., Zhang, R., Zhang, Y., 2016. A comparison of zircon U-Pb age results of the Red Clay sequence on the central Chinese Loess Plateau. Scientific Report 6, 29642.

Guo, Z.T., Peng, S.Z., Hao, Q.Z., Biscaye, P.E., Liu, T.S., 2001. Origin of the Miocene–Pliocene Red-Earth Formation at Xifeng in Northern China and implications for paleoenvironments. Palaeogeography Palaeoclimatology Palaeoecology 170, 11-26.

Guo, Z.T., Ruddiman, W.F., Hao, Q.Z., Wu, H.B., Qiao, Y.S., Zhu, R.X., Peng, S.Z., Wei, J.J., Yuan, B.Y., Liu, T.S., 2002. Onset of Asian desertification by 22 Myr ago inferred from loess deposits in China. Nature 416, 159-163.

Hao, Q.Z., Guo, Z.T., 2004. Magnetostratigraphy of a late Miocene-Pliocene loess-soil sequence in the western Loess Plateau in China. Geophysical Research Letters 31, L09209.

Harris, N., 2006. The elevation history of the Tibetan Plateau and its implications for the Asian monsoon. Palaeogeography, Palaeoclimatology, Palaeoecology 241, 4-15.

Heller, F., Liu, T.S., 1982. Magnetostratigraphical dating of loess deposits in China. Nature 300, 431-433.

Horton, B.K., Dupont-Nivet, G., Zhou, J., Waanders, G.L., Butler, R.F., Wang, J., 2004. Mesozoic-Cenozoic evolution of the Xining-Minhe and Dangchang basins, northeastern Tibetan Plateau: Magnetostratigraphic and biostratigraphic results. Journal of Geophysical Research-Solid Earth 109, B04402.

Hu, Z., Pan, B., Wang, J., Cao, B., Gao, H., 2012. Fluvial terrace formation in the eastern Fenwei Basin, China, during the past 1.2Ma as a combined archive of tectonics and climate change. Journal of Asian Earth Sciences 60, 235-245.

Hu, Z., Pan, B., Guo, L., Vandenberghe, J., Liu, X., Wang, J., Fan, Y., Mao, J., Gao, H., Hu, X., 2016. Rapid fluvial incision and headward erosion by the Yellow River along the Jinshaan gorge during the past 1.2 Ma as a result of tectonic extension. Quaternary Science Reviews 133, 1-14.

Hu, Z.B., Pan, B.T., Bridgland, D., Vandenberghe,

J., Guo, L.Y., Fan, Y.L., Westaway, R., 2017. The linking of the upper-middle and lower reaches of the Yellow River as a result of fluvial entrenchment. Quaternary Science Reviews 166, 324-338.

Huhma, H., Mänttäri, I., Peltonen, P., Kontinen, A., Halkoaho, T., Hanski, E., Hokkanen, T., Hölttä, P., Juopperi, H., Konnunaho, J., Layahe, Y., E., L., K., P., Pulkkinen, A., Sorjonen-Ward, P., Vaasjoki, M., Whitehouse, M., 2012. The age of the Archaean greenstone belts in Finland. Geological Survey of Finland. Geological Survey of Finland, Special Paper 54, 74-175.

Ji, J.L., Zheng, H.B., Liu, R., Huang, X., Jiang, F.C., 2004. Restudy on the stratigraphy of Mangshan loess. Marine Geology and Quaternary Geology 24, 101-108.

Jiang, F., Fu, J., Wang, S., Sun, D., Zhao, Z., 2007. Formation of the Yellow River, inferred from loess–palaeosol sequence in Mangshan and lacustrine sediments in Sanmen Gorge, China. Quaternary International 175, 62-70.

Kaakinen, A., 2005. A long terrestrial sequence in Lantian – a window into the late Neogene palaeoenvironments of Northern China. University of Helsinki, Helsinki, Finland.

Kaakinen, A., Lunkka, J.P., 2003. Sedimentation of the Late Miocene Bahe Formation and its implications for stable environments adjacent to Qinling mountains in Shaanxi, China. Journal of Asian Earth Sciences 22, 67-78.

Kaakinen, A., Passey, B.H., Zhang, Z., Liu, L., Pesonen, L.J., Fortelius, M., 2013. Stratigraphy and Paleoecology of the Classical Dragon Bone Localities of Baode County, Shanxi Province, In: Wang, X., Flynn, L.J., Fortelius, M. (Eds.), Fossil Mammals of Asia: Neogene Biostratigraphy and Chronology. Columbia University Press, New York, pp. 203-217.

Kapp, P., Pelletier, J.D., Rohrmann, A., Heermance, R., Russell, J., Ding, L., 2011. Wind erosion in the Qaidam basin, central Asia: Implications for tectonics, paleoclimate, and the source of the Loess Plateau. GSA Today 21, 4-10.

Knippertz, P., Stuut, J.-B.W., 2014. Mineral Dust: A Key Player in the Earth System. Springer, Netherlands.

Konert, M., Vandenberghe, J., 1997. Comparison of laser grain size analysis with pipette and sieve analysis: a solution for the underestimation of the clay fraction. Sedimentology 44, 523-535.

Kong, P., Jia, J., Zheng, Y., 2014. Time constraints for the Yellow River traversing the Sanmen Gorge. Geochemistry, Geophysics, Geosystems 15, 395-407.

Li, F., Wu, N., Rousseau, D.D., Dong, Y., Zhang, D., Pei, Y., 2014. Late Miocene–Pliocene paleoclimatic evolution documented by terrestrial mollusk populations in the western Chinese Loess Plateau. PLoS One 9, e95754.

Licht, A., Pullen, A., Kapp, P., Abell, J., Giesler, N., 2016a. Eolian cannibalism: Reworked loess and fluvial sediment as the main sources of the Chinese Loess Plateau. Geological Society of America Bulletin 128, 944-956.

Licht, A., Dupont-Nivet, G., Pullen, A., Kapp, P., Abels, H.A., Lai, Z., Guo, Z., Abell, J., Giesler, D., 2016b. Resilience of the Asian atmospheric circulation shown by Paleogene dust provenance. Nature communications 7, 12390.

Lin, A., Yang, Z., Sun, Z., Yang, T., 2001. How and when did the Yellow River develop its square bend? Geology 29, 951-954.

Liu, D., Ding, M., Gao, F., 1960. Cenozoic stratigraphic sections between Xi'an and Lantian. Geology Science 4, 199-208.

Liu, G.B., 1999. Soil conservation and sustainable agriculture on the Loess Plateau: Challenges and prospects. Ambio 28, 663-668.

Liu, L.P., Zheng, S.H., Cui, N., Wang, L.H., 2013. Myospalacines (Cricetidae, Rodentia) from the Miocene- Pliocene red clay section near Dongwan Village, Qin' an, Gansu, China and the classification of Myospalacinae. Vertebrata PalAsiatica 51, 211-241.

Liu, L.P., Zheng, S.H., Zhang, Z.Q., Wang, L.H., 2011. Late Miocene-Early Pliocene biostratigraphy and Miocene/ Pliocene boundary in the Dongwan section,Gansu. Vertebrata PalAsiatica 49, 229-240.

Liu, T.S., 1985. Loess and the Environment. China Ocean Press, Beijing.

Liu, T., Ding, Z., Rutter, N., 1999. Comparison of Milankovitch periods between continental loess and deep sea records over the last 2.5 Ma. Quaternary Science Reviews 18, 1205-1212.

Liu, W., Liu, Z., An, Z., Sun, J., Chang, H., Wang, N., Dong, J., Wang, H., 2014. Late Miocene episodic lakes in the arid Tarim Basin, western China. Proceedings of the National Academy of Sciences of the United States of America 111, 16292-16296.

Liu, X., Kutzbach, J.E., Liu, Z., An, Z., Li, L., 2003. The Tibetan Plateau as amplifier of orbital-scale variability of the East Asian monsoon. Geophysical Research Letters 30, 1839.

Lu, H.Y., Vandenberghe, J., An, Z.S., 2001. Aeolian origin and palaeoclimatic implications of the 'Red Clay' (north China) as evidenced by grain-size distribution. Journal of Quaternary Science 16, 89-97.

Ludwig, K.R., 2003. User's Manual for Isoplot 3.00 : a Geochronological Toolkit for Microsoft Excel, In: Ludwig, K.R. (Ed.), Berkeley CA.

Micheels, A., Bruch, A.A., Eronen, J., Fortelius, M., Harzhauser, M., Utescher, T., Mosbrugger, V., 2011. Analysis of heat transport mechanisms from

a Late Miocene model experiment with a fully-coupled atmosphere–ocean general circulation model. Palaeogeography Palaeoclimatology Palaeoecology 304, 337-350.

Muhs, D.R., Prospero, J.M., Baddock, M.C., Gill, T.E., 2014. Identifying Sources of Aeolian Mineral Dust: Present and Past, In: Knippertz, P., Stuut, J.-B.W. (Eds.), Mineral Dust: A Key Player in the Earth System. Springer, pp.51-74.

Nie, J., Peng, W., Möller, A., Song, Y., Stockli, D.F., Stevens, T., Horton, B.K., Liu, S., Bird, A., Oalmann, J., Gong, H., Fang, X., 2014. Provenance of the upper Miocene–Pliocene Red Clay deposits of the Chinese loess plateau. Earth and Planetary Science Letters 407, 35-47.

Nie, J., Stevens, T., Rittner, M., Stockli, D., Garzanti, E., Limonta, M., Bird, A., Ando, S., Vermeesch, P., Saylor, J., Lu, H., Breecker, D., Hu, X., Liu, S., Resentini, A., Vezzoli, G., Peng, W., Carter, A., Ji, S., Pan, B., 2015. Loess Plateau storage of Northeastern Tibetan Plateau-derived Yellow River sediment. Nature Communications 6, 8511.

Nie, J., Song, Y., King, J.W., 2016. A Review of Recent Advances in Red-Clay Environmental Magnetism and Paleoclimate History on the Chinese Loess Plateau. Frontiers of Earth Science 4, doi: 10.3389/feart.2016.00027.

Nugteren, G., Vandenberghe, J., 2004. Spatial climatic variability on the Central Loess Plateau (China) as recorded by grain size for the last 250 kyr. Global and Planetary Change 41, 185-206.

Penck, 1931. Zentral-Asien. Zeitschr. Gesell. Erdk. Berlin, 1-13.

Prins, M.A., Postma, G., Weltje, G.J., 2000. Controls on terrigenous sediment supply to the Arabian Sea during the late Quaternary: the Makran continental slope. Marine Geology 169, 351-371.

Prins, M.A., Vriend, M., 2007. Glacial and interglacial eolian dust dispersal patterns across the Chinese Loess Plateau inferred from decomposed loess grain-size records. Geochemistry, Geophysics, Geosystems 8, Q07Q05, doi:10.1029/2006GC001563.

Prins, M.A., Vriend, M., Nugteren, G., Vandenberghe, J., Lu, H., Zheng, H., Jan Weltje, G., 2007. Late Quaternary aeolian dust input variability on the Chinese Loess Plateau: inferences from unmixing of loess grain-size records. Quaternary Science Reviews 26, 230-242.

Prins, M.A., Zheng, H., Beets, K., Troelstra, S., Bacon, P., Kamerling, I., Wester, W., Konert, M., Huang, X., Ke, W., Vandenberghe, J., 2009. Dust supply from river floodplains: the case of the lower Huang He (Yellow River) recorded in a loess-palaeosol sequence from the Mangshan Plateau. Journal of Quaternary Science 24, 75-84.

Prospero, J.M., Blades, E., Naidu, R., Mathison, G., Thani, H., Lavoie, M.C., 2008. Relationship between African dust carried in the Atlantic trade winds and surges in pediatric asthma attendances in the Caribbean. International Journal of Biometeorology 52, 823-832.

Prospero, J.M., Bullard, J.E., Hodgkins, R., 2012. High-latitude dust over the North Atlantic: inputs from Icelandic proglacial dust storms. Science 335, 1078-1082.

Pullen, A., Kapp, P., McCallister, A.T., Chang, H., Gehrels, G.E., Garzione, C.N., Heermance, R.V., Ding, L., 2011. Qaidam Basin and northern Tibetan Plateau as dust sources for the Chinese Loess Plateau and paleoclimatic implications. Geology 39, 1031-1034.

Pye, K., 1995. The nature, origin and accumulation of loess. Quaternary Science Reviews 14, 653-667.

Pye, K., Zhou, L.-P., 1989. Late Pleistocene and Holocene aeolian dust deposition in North China and the Northwest Pacific Ocean. Palaeogeography, Palaeoclimatology, Palaeoecology 73, 11-23.

Qiang, X., An, Z., Song, Y., Chang, H., Sun, Y., Liu, W., Ao, H., Dong, J., Fu, C., Wu, F., Lu, F., Cai, Y., Zhou, W., Cao, J., Xu, X., Ai, L., 2011. New eolian red clay sequence on the western Chinese Loess Plateau linked to onset of Asian desertification about 25 Ma ago. Science China Earth Sciences 54, 136-144.

Qiang, X.K., An, Z.S., Li, H.M., Chang, H., Song, Y.G., 2005. Magnetic properties of Jiaxian red clay sequences from northern Chinese Loess Plateau and its paleoclimatic significance. Science in China Series D–Earth Sciences 48, 1234-1245.

Qiu, F., Zhou, L., 2015. A new luminescence chronology for the Mangshan loess-palaeosol sequence on the southern bank of the Yellow River in Henan, central China. Quaternary Geochronology 30, 24-33.

Raymo, M.E., Ruddiman, W.F., 1992. Tectonic forcing of late Cenozoic climate. Nature 359, 117-122.

Rits, D.S., van Balen, R.T., Prins, M.A., Zheng, H.B., 2017. Evolution of the alluvial fans of the Luo River in the Weihe Basin, central China, controlled by faulting and climate change - A reevaluation of the paleogeographical setting of Dali Man site. Quaternary Science Reviews 166, 339-351.

Rittner, M., Vermeesch, P., Carter, A., Bird, A., Stevens, T., Garzanti, E., Andò, S., Vezzoli, G., Dutt, R., Xu, Z., Lu, H., 2016. The provenance of Taklamakan desert sand. Earth and Planetary Science Letters 437, 127-137.

Roe, G., 2009. On the interpretation of Chinese loess as a paleoclimate indicator. Quaternary Research 71, 150-161.

Rosa, D.R.N., Finch, A.A., Andersen, T., Inverno, C.M.C., 2009. U-Pb geochronology and Hf isotope ratios of magmatic zircons from the

Iberian Pyrite Belt. Mineralogy and Petrology 95, 47-69.

Schroedter-Homscheidt, M., Oumbe, A., Benedetti, A., Morcrette, J.-J., 2013. Aerosols for Concentrating Solar Electricity Production Forecasts: Requirement Quantification and ECMWF/MACC Aerosol Forecast Assessment. Bulletin of the American Meteorological Society 94, 903-914.

Smalley, I., O'Hara-Dhand, K., Wint, J., Machalett, B., Jary, Z., Jefferson, I., 2009. Rivers and loess: The significance of long river transportation in the complex event-sequence approach to loess deposit formation. Quaternary International 198, 7-18.

Song, B., Ji, J., Wang, C., Xu, Y., Zhang, K., 2017. Intensified aridity in the Qaidam Basin during the Middle Miocene: constraints from ostracod, stable isotope, and weathering records. Canadian Journal of Earth Sciences 54, 242-256.

Spandler, C., Pettke, T., Rubatto, D., 2011. Internal and External Fluid Sources for Eclogite-facies Veins in the Monviso Meta-ophiolite, Western Alps: Implications for Fluid Flow in Subduction Zones. Journal of Petrology 52, 1207-1236.

Stevens, T., Carter, A., Watson, T.P., Vermeesch, P., Andò, S., Bird, A.F., Lu, H., Garzanti, E., Cottam, M.A., Sevastjanova, I., 2013. Genetic linkage between the Yellow River, the Mu Us desert and the Chinese Loess Plateau. Quaternary Science Reviews 78, 355-368.

Stevens, T., Palk, C., Carter, A., Lu, H., Clift, P.D., 2010. Assessing the provenance of loess and desert sediments in northern China using U-Pb dating and morphology of detrital zircons. Geological Society of America Bulletin 122, 1331-1344.

Stuut, J.-B.W., Prins, M.A., Schneider, R.R., Weltje, G.J., Jansen, J.H.F., Postma, G., 2002. A 300-kyr record of aridity and wind strength in southwestern Africa: inferences from grain-size distributions of sediments on Walvis Ridge, SE Atlantic. Marine Geology 180, 221-233.

Stuut, J.-B.W., Temmesfeld, F., De Deckker, P., 2014. A 550 ka record of aeolian activity near North West Cape, Australia: inferences from grain-size distributions and bulk chemistry of SE Indian Ocean deep-sea sediments. Quaternary Science Reviews 83, 83-94.

Sugimoto, N., Matsui, I., Shimizu, A., Uno, I., Asai, K., Endoh, T., Nakajima, T., 2002. Observation of dust and anthropogenic aerosol plumes in the Northwest Pacific with a two-wavelength polarization lidar on board the research vessel Mirai. Geophysical Research Letters 29, 1901.

Sun, D., Bloemendal, J., Rea, D.K., Vandenberghe, J., Jiang, F., An, Z., Su, R., 2002. Grain-size distribution function of polymodal sediments in hydraulic and aeolian environments, and numerical partitioning of the sedimentary components. Sedimentary Geology 152, 263-277.

Sun, D., Liu, D., Chen, M., An, Z., John, S., 1997. Magnetostratigraphy and palaeoclimate of Red Clay sequences from Chinese Loess Plateau. Science in China Series D: Earth Sciences 40, 337-343.

Sun, D., Shaw, J., An, Z., Cheng, M., Yue, L., 1998. Magnetostratigraphy and paleoclimatic interpretation of a continuous 7.2 Ma Late Cenozoic Eolian sediments from the Chinese Loess Plateau. Geophysical Research Letters 25, 85-88.

Sun, J., 2002. Provenance of loess material and formation of loess deposits on the Chinese Loess Plateau. Earth and Planetary Science Letters 203, 845-859.

Sun, J., Zhang, M., Liu, T., 2001. Spatial and temporal characteristics of dust storms in China and its surrounding regions, 1960-1999: Relations to source area and climate. Journal of Geophysical Research: Atmospheres 106, 10325-10333.

Sun, J.M., Gong, Z.J., Tian, Z.H., Jia, Y.Y., Windley, B., 2015. Late Miocene stepwise aridification in the Asian interior and the interplay between tectonics and climate. Palaeogeography Palaeoclimatology Palaeoecology 421, 48-59.

Sun, Y., Lu, H.Y., An, Z.S., 2006. Grain size of loess, palaeosol and Red Clay deposits on the Chinese Loess Plateau: Significance for understanding pedogenic alteration and palaeomonsoon evolution. Palaeogeography Palaeoclimatology Palaeoecology 241, 129-138.

Swap, R., Garstang, M., Greco, S., Talbot, R., Kallberg, P., 1992. Saharan dust in the Amazon Basin. Tellus B 44, 133-149.

Tedford, R.H., Qiu, Z.-X., Ye, J., 2013. Cenozoic Geology of the Yushe Basin, In: Tedford, R.H., Qiu, Z.-X., Flynn, L.J. (Eds.), Late Cenozic Yushe Basin, Shanxi Province, China: Geology and Fossil Mammals. Volume I: History, Geology, and Magnetostratigraphy, Vertebrate Paleobiology and Paleoanthropology. Springer.

Teilhard de Chardin, P., Young, C.C., 1931. Fossil mammals from the Late Cenozoic of Northern China. Palaeontologia Sinica 9, 1-67.

Tsoar, H., Pye, K., 1987. Dust transport and the question of desert loess formation. Sedimentology 34, 139-153.

Tysmans, D., Claeys, P., Deriemaeker, L., Maes, D., Finsy, R., Van Molle, M., 2006. Size and shape analysis of sedimentary grains by automated dynamic image analysis. Particle & Particle Systems Characterization 23, 381-387.

UCAR, 2006. China Monthly Station Precipitation and Temperature, 1951–1990.

Van Achterbergh, E., Ryan C., Jackson, S., Griffin, W., 2001. Data reduction software for LA-ICP-

MS, In: P., S. (Ed.), Laser-Ablation ICPMS in the Earth Sciences – Principles and applications. Mineralogical Association of Canada short course series, St John, Newfoundland, pp. 239-243.

Vandenberghe, J., Lu, H.Y., Sun, D.H., van Huissteden, J., Konert, M., 2004. The late Miocene and Pliocene climate in East Asia as recorded by grain size and magnetic susceptibility of the Red Clay deposits (Chinese Loess Plateau). Palaeogeography Palaeoclimatology Palaeoecology 204, 239-255.

Vermeesch, P., 2012. On the visualisation of detrital age distributions. Chemical Geology 312-313, 190-194.

Vermeesch, P., 2013. Multi-sample comparison of detrital age distributions. Chemical Geology 341, 140-146.

Vriend, M., Prins, M.A., 2005. Calibration of modelled mixing patterns in loess grain-size distributions: an example from the north-eastern margin of the Tibetan Plateau, China. Sedimentology 52, 1361-1374.

Vriend, M., Prins, M.A., Buylaert, J.P., Vandenberghe, J., Lu, H.Y., 2011. Contrasting dust supply patterns across the north-western Chinese Loess Plateau during the last glacial-interglacial cycle. Quaternary International 240, 167-180.

Wang, B., Zheng, H.B., He, Z., Wang, P., Kaakinen, A., Zhou, X.Y., 2014. Middle Miocene eolian sediments on the southern Chinese Loess Plateau dated by magnetostratigraphy. Palaeogeography Palaeoclimatology Palaeoecology 411, 257-266.

Wang, B., Kaakinen, A., Clift, P.D., 2017. Tectonic controls of the onset of aeolian deposits in Chinese Loess Plateau – a preliminary hypothesis. International Geology Review, doi: 10.1080/00206814.2017.1362362.

Wang, S., 2002. Sedimentary records of environmental evolution in the Sanmen Lake Basin and the Yellow River running through the Sanmenxia Gorge eastward into the sea. Science in China Series D 45, 595-608.

Wang, S.B., Jiang, F.C., Fu, J.L., Li, C.Z., Cai, Y., Yao, H.T., Qiao, Y.S., Zhang, Z.S., Li, Y.J., 2013. Some knowledge of the formation of the Yellow River. Quaternary Sciences 33, 705-714.

Wang, Y., Cheng, H., Edwards, R.L., Kong, X., Shao, X., Chen, S., Wu, J., Jiang, X., Wang, X., An, Z., 2008. Millennial- and orbital-scale changes in the East Asian monsoon over the past 224,000 years. Nature 451, 1090-1093.

Weltje, G.J., 1997. End-member modeling of compositional data: Numerical-statistical algorithms for solving the explicit mixing problem. Mathematical Geology 29, 503-549.

Weltje, G.J., Prins, M.A., 2003. Muddled or mixed? Inferring palaeoclimate from size distributions of deep-sea clastics. Sedimentary Geology 162, 39-62.

Weltje, G.J., Prins, M.A., 2007. Genetically meaningful decomposition of grain-size distributions. Sedimentary Geology 202, 409-424.

Wu, F., Fang, X., Herrmann, M., Mosbrugger, V., Miao, Y., 2011. Extended drought in the interior of Central Asia since the Pliocene reconstructed from sporopollen records. Global and Planetary Change 76, 16-21.

Xiao, G.Q., Zong, K.Q., Li, G.J., Hu, Z.C., Dupont-Nivet, G., Peng, S.Z., Zhang, K.X., 2012. Spatial and glacial-interglacial variations in provenance of the Chinese Loess Plateau. Geophysical Research Letters 39, L20715.

Yuan, B.Y., Tang, G.A., Zhou, L.P., Hao, Q.Z., Li, F.Y., Lu, Z.C., 2012. Control action on the geomorphic differentiation of loess plateau and formation of yellow river by Cenozoic tectogenesis. Quaternary Sciences 32, 830-838.

Zdansky, O., 1923. Fundorte der Hipparion-Fauna um Pao-Te-Hsien in NW-Shansi. Bulletin of the Geological Survey of China 5, 69-82.

Zhang, H., Lu, H., Xu, X., Liu, X., Yang, T., Stevens, T., Bird, A., Xu, Z., Zhang, T., Lei, F., Feng, H., 2016. Quantitative estimation of the contribution of dust sources to Chinese loess using detrital zircon U-Pb age patterns. Journal of Geophysical Research: Earth Surface 121, 2085-2099.

Zhang, R., Jiang, D., Zhang, Z., Yu, E., 2015. The impact of regional uplift of the Tibetan Plateau on the Asian monsoon climate. Palaeogeography, Palaeoclimatology, Palaeoecology 417, 137-150.

Zhang, Y.P., Huang, W.B., Tang, Y.J., Ji, H.X., You, Y.Z., Tong, Y.S., Ding, S.Y., Huang, X.S., Zheng, J.J., 1978. Cainozoic of the Lantian area, Shaanxi. Memoirs of Institute of Vertebrate Paleontology and Paleoanthropology, Academia Sinica Special Publication A 14, 1-64.

Zhang, Z., Kaakinen, A., Liu, L., Lunkka, J.P., Sen, S., Gose, W.A., Qiu, Z., Zheng, S., Fortelius, M., 2013. Mammalian Biochronology of the Late Miocene Bahe Formation, In: Wang, X., Flynn, L.J., Fortelius, M. (Eds.), Fossil Mammals of Asia: Neogene Biostratigraphy and Chronology. Columbia University Press, New York, pp. 187-202.

Zhang, Z., Wang, H., Guo, Z., Jiang, D., 2007. What triggers the transition of palaeoenvironmental patterns in China, the Tibetan Plateau uplift or the Paratethys Sea retreat? Palaeogeography, Palaeoclimatology, Palaeoecology 245, 317-331.

Zhang, Z., Wang, S., Yang, X., Jiang, F., Shen, J., Li, X., 2004. Evidence of a geological event and environmental change in the catchment area of the Yellow River at 0.15Ma. Quaternary International 117, 35-40.

Zheng, H., Huang, X., Ji, J., Liu, R., Zeng, Q., Jiang, F., 2007. Ultra-high rates of loess sedimentation

at Zhengzhou since Stage 7: Implication for the Yellow River erosion of the Sanmen Gorge. Geomorphology 85, 131-142.
Zheng, H., Wei, X., Tada, R., Clift, P.D., Wang, B., Jourdan, F., Wang, P., He, M., 2015. Late Oligocene-early Miocene birth of the Taklimakan Desert. Proceedings of the National Academy of Sciences of the United States of America 112, 7662-7667.
Zhu, Y., Zhou, L., Mo, D., Kaakinen, A., Zhang, Z., Fortelius, M., 2008. A new magnetostratigraphic framework for late Neogene Hipparion Red Clay in the eastern Loess Plateau of China. Palaeogeography Palaeoclimatology Palaeoecology 268, 47-57.